Peer-reviewed version available at C 2018, 4, 63; doi:10.3390/c4040063

Review

A Review on Synthesis and Characterization of Biomass-Derived Carbons for Adsorption of Emerging Contaminants from Water

Jorge Bedia*, Manuel Peñas-Garzón, Almudena Gómez-Avilés, Juan Jose Rodríguez and Carolina Belver

Departamento de Ingeniería Química, Facultad de Ciencias, Universidad Autónoma de Madrid, Campus Cantoblanco, E-28049 Madrid, Spain; manuel.pennas@uam.es; almudena.gomeza@uam.es; juanjo.rodriguez@uam.es, carolina.belver@uam.es.

* Correspondence: jorge.bedia@uam.es; Tel.: +34-91-497-2911

Abstract: This review analyzes the synthesis and characterization of biomass-derived carbons for adsorption of emerging contaminants from water. The study begins with the definition and different types of emerging contaminants more often founded in water streams and the different technologies available for their removal including adsorption. It also describes the biomass sources that could be used for the synthesis of biochars and activated carbons. The characterization of the adsorbents and the different approaches that could be employed for the study of the adsorption processes are also detailed. Finally, the work reviews in detail some studies of the literature focused on the adsorption of emerging contaminants on biochars and activated carbons synthesized from biomass precursors.

Keywords: Adsorption; Emerging contaminants; Biomass; Biochar; Activated carbon.

1. Emerging contaminants

Emerging contaminants (ECs) are those compounds found in wastewater in low concentrations as a consequence of the new habits of consume developed in our society. The discharge limitations of these compounds, due to their very recent appearance in the environment, are not completely or not at all regulated, which can result in real hazards to the human health and environment [1,2]. The list of compounds considered as emerging contaminants includes many different substances such as, pharmaceutical and personal care products (PPCPs), drugs of abuse, food additives, plasticizers, pesticides, among others [3]. Table 1 summarizes the categories, families and most representative examples of ECs usually found in wastewater. Their low concentration, typically in the range from $ng \cdot L^{-1}$ up to $\mu g \cdot L^{-1}$, makes their detection and elimination in conventional water treatment plants very difficult since these are not designed for treating so low concentrations [4]. Only the development and greater availability of new and more sensible analytical techniques such as liquid chromatography coupled with mass spectrometry (LC-MS) has allowed the detection of this new type of pollutants. This fact, together with the development of increasingly restrictive governmental regulations regarding the permitted concentrations of these compounds in effluents, has significantly increased the studies aimed to the removal of ECs from wastewater.

The technologies available for the removal of ECs from wastewaters can be broadly classified in three subcategories, namely biological treatments, advanced oxidation processes (AOPs) and phase-changing technologies [5]. Among biological treatments, activated sludge, in both aerobic and anaerobic conditions, is the most commonly studied due to its higher effectiveness [6]. Other biological process used for the degradation of ECs are soil filtration [7] and biological filtration [8]. The efficiency of the biological processes has been increased when combined with phase-changing processes in membrane bioreactors [9] or even electrochemical membrane bioreactors (EMBR) [10,11]. The main problem for using biological processes for the removal of ECs is their significant toxicity towards microorganism. Advanced oxidation processes (AOPs) use the high reactivity of $HO^{\bullet}$

radicals in oxidation reactions which are able to achieve the mineralization of the pollutants [12]. These processes include Fenton, sonolysis, ozonation, electrochemical oxidation and photocatalysis. Finally, phase changing-technologies are those processes in which the contaminants are transferred from one phase (liquid phase in the case of water treatment) to another (e.g. solid). The main examples of this type of technology include adsorption and membrane technology. Figure 1 summarizes the technologies available for the removal of ECs from wastewater.

Table 1. ECs usually found in wastewater (Adapted from [13]).

Main categories	Family	Most representative examples
Drugs and Pharmaceuticals	antibiotics/antibacterials	tetracycline, sulfamethoxazole, amoxicillin, ofloxacin
	steroids	17β-estradiol, testosterone
	β-blocker	propranolol, salbutamol, atenolol
	nonsteroidal anti-inflammatory drugs (NSAID)	ibuprofen, naproxen, ketoprofen, diclofenac
	antiepileptic/anticonvulsants	gabapentin, carbamazepine
	antidepressant/hypnotic	diazepam, venlafaxine, amitriptyline, dosulepin, meprobanate
	analgesic	morphine, antipyrine, paracetamol
	hypertension	valsartan
	lipid regulation	bezafibrate, simvastatin, clofibric acid
	erectile dysfunction	sildenafil
Stimulant and generally illegal drugs	hallucinogen	3,4-Methylenedioxymethamphetamine (MDMA), 3,4-Methylenedioxy-N-ethylamphetamine (MDEA), 3,4-Methylenedioxyamphetamine (MDA)
	stimulant	amphetamine, cocaine, benzylpiperazine
	human indicator	caffeine, nicotine
Personal care products	preservative	methylparaben, propylparaben
	sunscreen agent	1-benzophenone, homosalate
	disinfectants/antiseptic	chloramines, chlorine, chlorine dioxide, chlorhexidine digluconate, triclosan
	fragrances	musk xylol, tonalide
Pesticides/Herbicides	organohalogenated compounds	dichlorodiphenyltrichloroethane (DDT), lindane, vinclozolin, clopyralid
	nitrogen containing	simazine, phenylurea, atrazine, glyphosate, diuron
Plasticizers [14]	general purpose	phthalates
	low volatility	trimetallites
	flame resistant	epoxides

Among the different technologies used for the elimination of ECs from water effluents in this review we focus on adsorption processes. Adsorption has numerous advantages such as ease of implementation, the use and handling of chemical products is not necessary, and its cost is relatively low [15,16]. In the literature numerous adsorbents have been used including clays [17], zeolites [18] or metal organic frameworks [19], but certainly among all carbon-based materials have been the most extensively studied [20,21]. The preparation of carbonaceous adsorbents from biomass waste has also important added advantages, such as an effective management of the waste and lower synthesis cost.

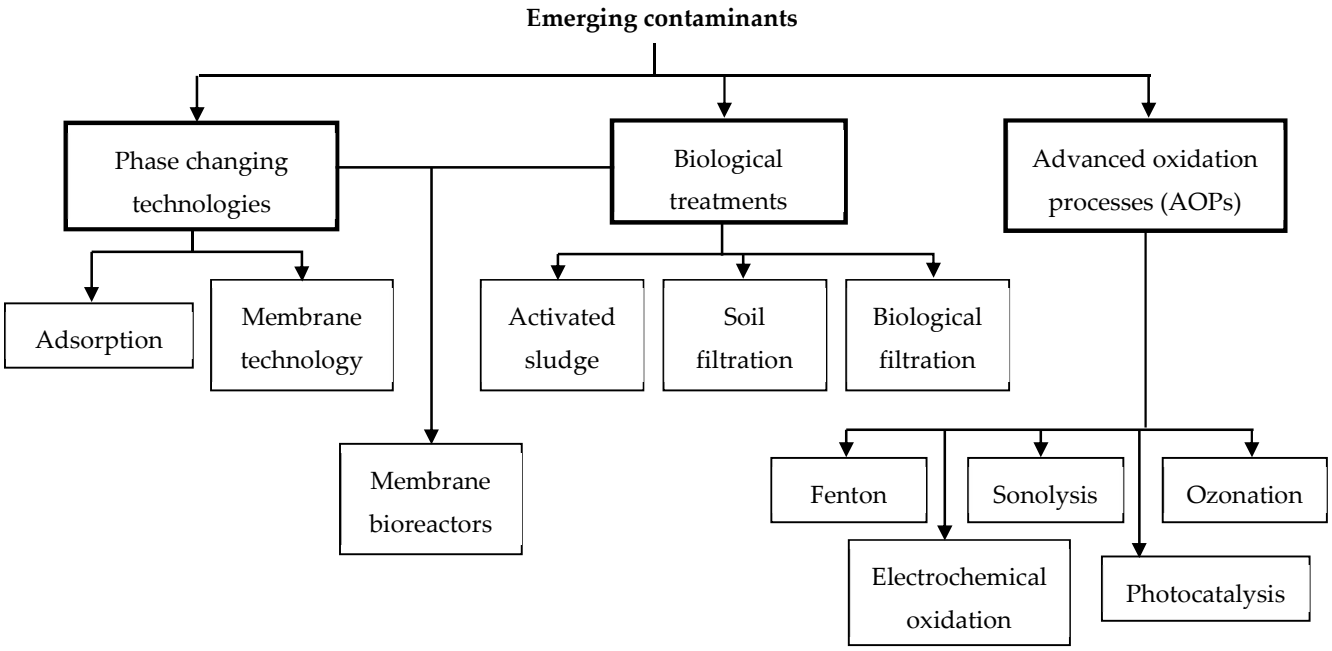

Figure 1. Technologies available for the removal of ECs from wastewater.

2. Biomass feedstocks

Biomass use sunlight and nutrients to grow and generate key components such as, carbohydrates, lipids and proteins, which can be converted to biofuels and different products in the frame of biorefinery concept [22–24]. Biomass covers all forms of organic material, including plants both living and in waste form, and animal waste products. It can be divides in two different categories: (i) waste material, or (ii) dedicated energy crops [25]. Biomass waste materials include agricultural residues, municipal solid waste (MSW), food processing waste and animal manure among others. The value that can be obtained from these wastes cannot be ignored as a valuable bioenergy source. If effectively harnessed, biomass wastes can be used as raw material for the synthesis of high value solid products and/or chemicals, as well as, reduce the energy consumption from nonrenewable fossil fuel sources. Furthermore, the use of solid waste materials would also save landfill space and increase the value of the biomass resource [26]. The different types of biomass feedstocks are summarized in Figure 2 and briefly described below.

Dedicated Energy Crops

Dedicated energy crops can be grown more or less arid lands, which are not fertile enough for traditional crops but it can be used to obtain biomass [27,28]. There exist two main types of dedicated energy crops: herbaceous and woody. The former are grasses harvested annually including bamboo, wheatgrass, sorghum, among many others. The latter are constituted by fast-growing hardwood trees such as, poplar, willow, maple, walnut and so on.

Forestry Residues

These feedstocks can be categorized in forest residues obtained after logging timber or complete trees grown specifically for biomass collection [29,30]. Forest residues could be also obtained from the excess biomass on the high extension forests. This action reduces the risk of fire and pests, and enhanced the forest vitality, productivity and resilience.

Peer-reviewed version available at C 2018, 4, 63; doi:10.3390/c4040063

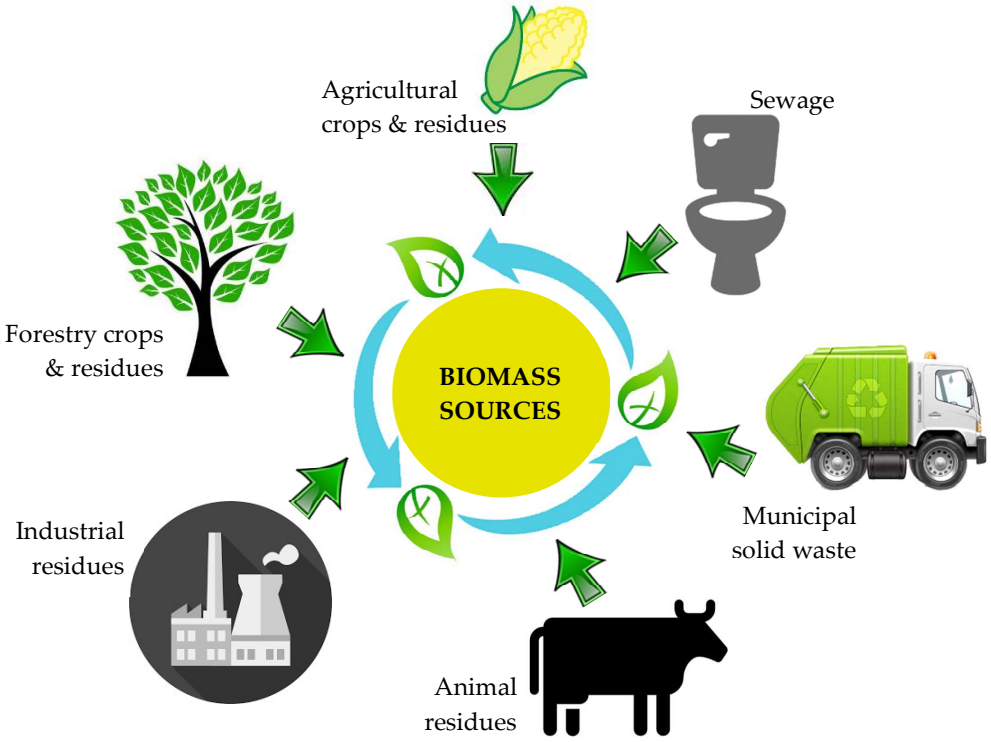

Figure 2. Different types of biomass feedstocks.

Agricultural Crop Residue

The use of agricultural biomass residues to produce biofuels, energy and high value materials can achieve interesting environmental and socio-economic benefits. Agricultural crop residues, which include the wheat, barley, rye, oat, maize, rice, rapeseed and sunflower, are abundant, diverse, and widely distributed [31,32]. The benefits of the sale of these residues can produce complementary incomes supporting to local economy.

Algae

Algae as feedstocks include the different biomass that grows in aquatic environment, covering microalgae, seaweed and even cyanobacteria. Algae can grow in different type of waters including fresh, saline, brackish water and even in wastewater from different sources, such as, agricultural water, treated industrial wastewater; aquaculture wastewater, water from oil and gas drilling operations, and so on. Due to this, they can be considered a very promising biomass feedstock with a very interesting growth potential in the near future [33,34].

Municipal solid wastes

Municipal solid wastes (MSW) are the materials discarded in urban areas, including predominantly household waste. MSW is a heterogeneous biomass feedstock mainly composed of food waste, rests of paper, wood trimmings and some textiles. A significant proportion of MSW is derived from fossil resources, such as rubber, plastics, and some fabrics [35]. The use of MSW as raw materials for bioenergy can reduce the huge volume of residential and commercial waste addressed to landfills.

Wet Waste

Wet waste biomass includes food wastes, sewage sludge from municipal wastewater treatment plants, manure slurries, different organic wastes from industrial processes and the biogas obtained

by the decomposition of organic matter in the absence of oxygen of any of the above feedstock resources. The transformation of these waste into energy or high-value products can generate additional incomes for rural areas, besides to reduce waste-disposal problems [36,37].

3. Synthesis of biomass-derived carbons

In general terms, carbon-based adsorbents can be synthesized from any precursor with a high proportion on carbon in its composition. Therefore, biomass materials are ideal precursor of carbon adsorbent, i.e. biochars or activated carbons. The difference between biochar and biomass-derived activated carbon is somewhat diffuse. In this study, we are going to consider biochar those materials obtained from biomass not submitted to an activation stage, while activated carbons are necessary obtained from an activation stage. The literature contains many studies about the synthesis of carbon adsorbent from biomass agricultural waste, such as olive stones [38–40], rice husk [41,42], coconut husks [43–46] or bamboo [47,48]. Furthermore, many studies have focused also in the synthesis of carbon materials from biomass industrial wastes including lignin (a by-product of the papermaking industry) [49–53], Tara gum (generated in the food industry) [54], wood wastes or sawdust (from furniture industry) [55,56], and so on.

Figure 3 schematizes the synthesis routes to biochars and activated carbons from biomass. Biochar synthesis usually consist of a carbonization step, while activated carbon synthesis can be performed by two well-known different ways, namely physical activation and chemical activation, giving rise to higher porous development. In the last years, alternative synthesis procedures with the aim of energy and/or chemical savings have been proposed. Thus, non-conventional methods such as microwave heating [57–60] and hydrothermal carbonization treatment [61–63] are being analyzed for both biochars and activated carbon synthesis. It is worth mentioning that the porosity, surface chemistry and yields of the carbon-based adsorbents synthesized are highly dependent on the biomass composition feedstock and the conditions used in the synthesis.

3.1. Biochars

Biochar was firstly used for soil amendment, due to its advantages of carbon sequestration, soil fertility improvement, pollution remediation, and agricultural by-product/waste recycling [64]. Nowadays, biochars applications include catalysis, energy storage and environmental protection [65], highlighting the use of biochar as adsorbent [66].

As aforementioned, the synthesis of biochars is usually performed by a single carbonization step. The biomass is heated in inert atmosphere, to avoid its combustion, up to temperatures in the range of 500 to 800 ºC and maintained at the desired temperature for a specific time. Finally, the biochar is cooled to room temperature also under inert atmosphere. Without doubt the most important parameter affecting the porous texture of biochars is the carbonization temperature. Chen et al reported [67] an interesting analysis of the effect of the carbonization temperature on the surface area of biochars obtained from different biomass resources (Figure 4). At low carbonization temperature (<400 ºC), no significant porous development is achieved probably as a consequence of the incomplete removal of volatile matter [68]. However, a further increase of the carbonization temperature beyond 400 ºC up to 900 ºC results in a significant increase of the surface area influenced by the biomass precursor and the carbonization conditions. This rise is due to the release of most of the volatile matter resulting in the formation of new porosity [69,70]. Carbonization temperatures higher than 900 ºC produce a decrease in the surface area. This could be due to pore widening and coalescence, structural reordering and also to the blocking of part of the porous structure by the melting and fusion of the ashes from the biomass feedstock [71]. Other explanations of this surface area reduction include the collapse of the microporosity [72] or the reordering of the carbon structure to graphite microcrystalline domains [73].

Peer-reviewed version available at C 2018, 4, 63; doi:10.3390/c4040063

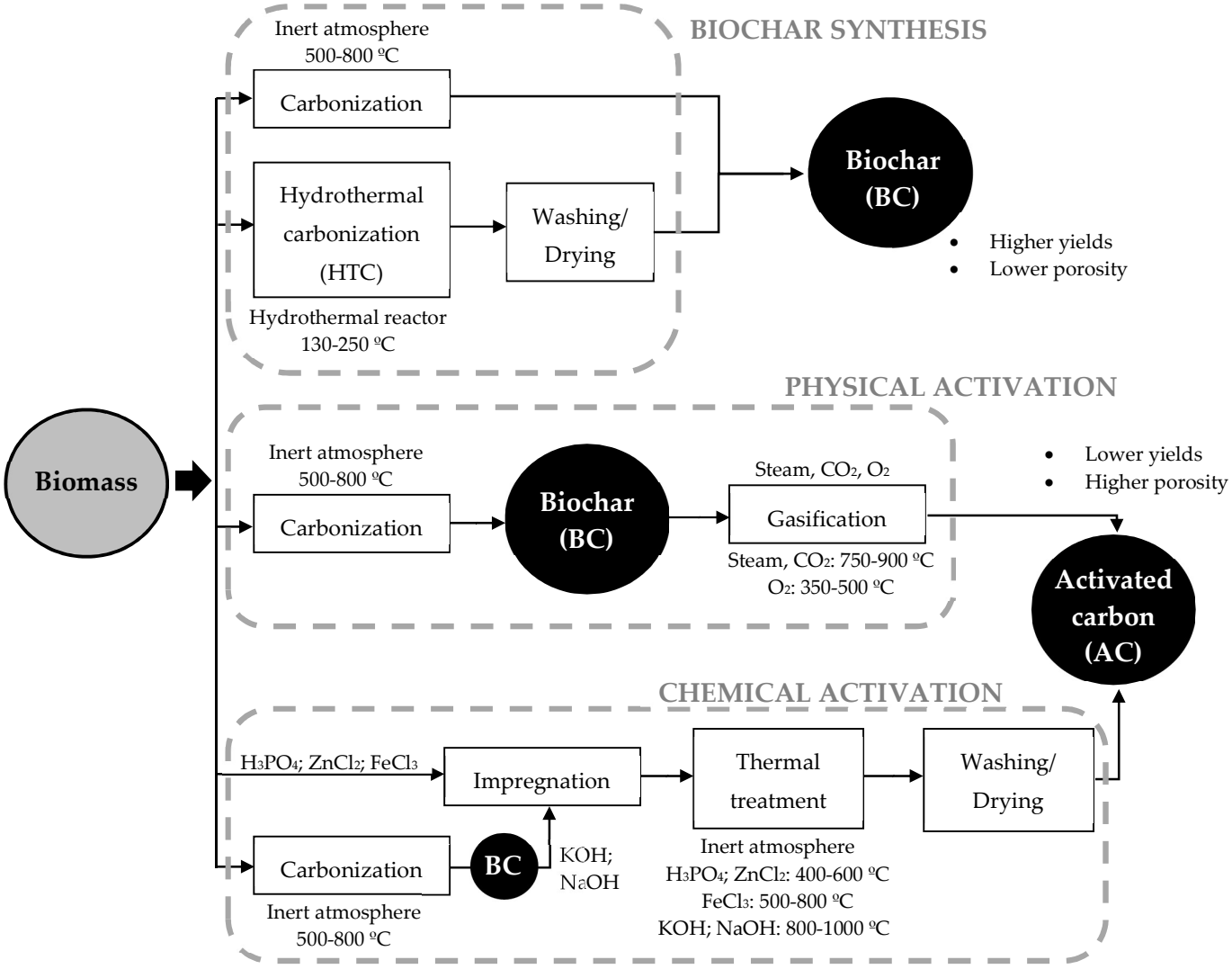

Figure 3. Synthesis routes to biochars and activated carbons from biomass.

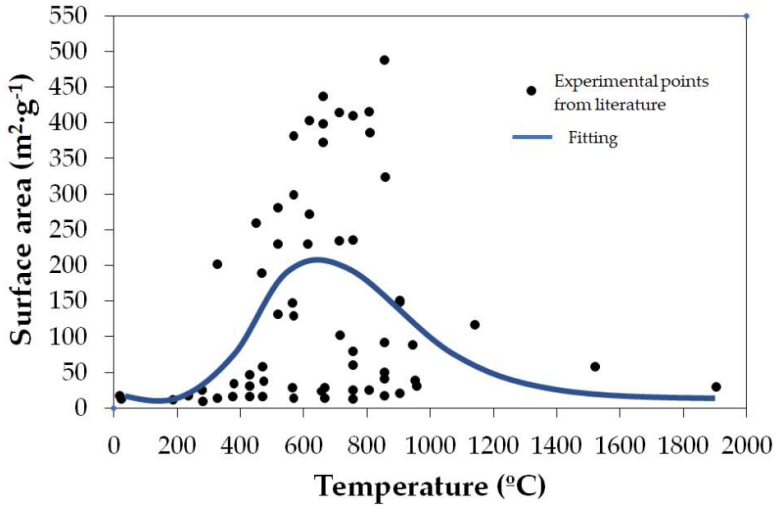

Figure 4. evolution of the surface area of biochars obtained from different biomass resources with the carbonization temperature (adapted from [67]).

The evolution of the functional groups upon carbonization of biomass could have also a very significant effect in the adsorptive properties. Usually, the H/C and O/C ratios of raw biomass were in the ranges of 1.4–1.8 and 0.55–0.75, respectively, confirming the high aliphatic content and low aromaticity of biomass [74]. Carbonization results in a decrease in these ratios, more significant at higher temperatures [71,75]. At carbonization temperatures lower than 500 °C, this reduction is due release of water, carbon dioxide and monoxide and other volatile products produced by dehydration, decarboxylation and decarbonylation of biomass. At carbonization temperature higher than 500 °C the dehydrogenation and demethanation of biomass results in a reduction of the H/C more accentuated than the O/C ratio [71].

In the last years, increasing attention is being paid to the synthesis of biochar by *hydrothermal carbonization* [61,62]. Biochar synthesis by this methodology offers significant advantages. The relatively low operation temperature and the absence of a drying step reduce considerably the energy consumption, and therefore, the cost of the synthesis. Like in a conventional carbonization/pyrolysis process, hydrothermal carbonization of biomass yields liquid (bio-oil), gaseous (low molecular weight hydrocarbons) and solid products (biochar), being the proportions and characteristics of these products dependent on conditions of the treatment and the biomass feedstock [76]. This synthesis is usually performed in water medium inside closed vessel at temperatures in the range of 130 to 250 ºC for about 2–24 h. During the hydrothermal carbonization dehydration and decarboxylation reactions take place in an exothermic process [62].

In the case of water purification, to effectively enhanced the adsorption capacity of organic pollutants on biochar adsorbents, these should present a well-developed porosity and hydrophobic surfaces. In the case of adsorption of inorganic or polar organic contaminants, the presence of oxygen-surface groups is needed to increase electrostatic attraction [77]. Regrettably, biochars usually show moderated to low surface area and a limited amount of surface functional groups, which limit their practical applications. With the aim of improving the biochar's adsorption capacities different modifications have been proposed (Figure 5). Among them, the further activation process of biochar favors the development of porosity. Actually, this approach transforms biochar into activated carbons, which will be analyzed in more detail in the following section of this review. The surface chemistry of the biochars can be modified by doping with heteroatoms, including N, P, S and metal oxide from different reagents.

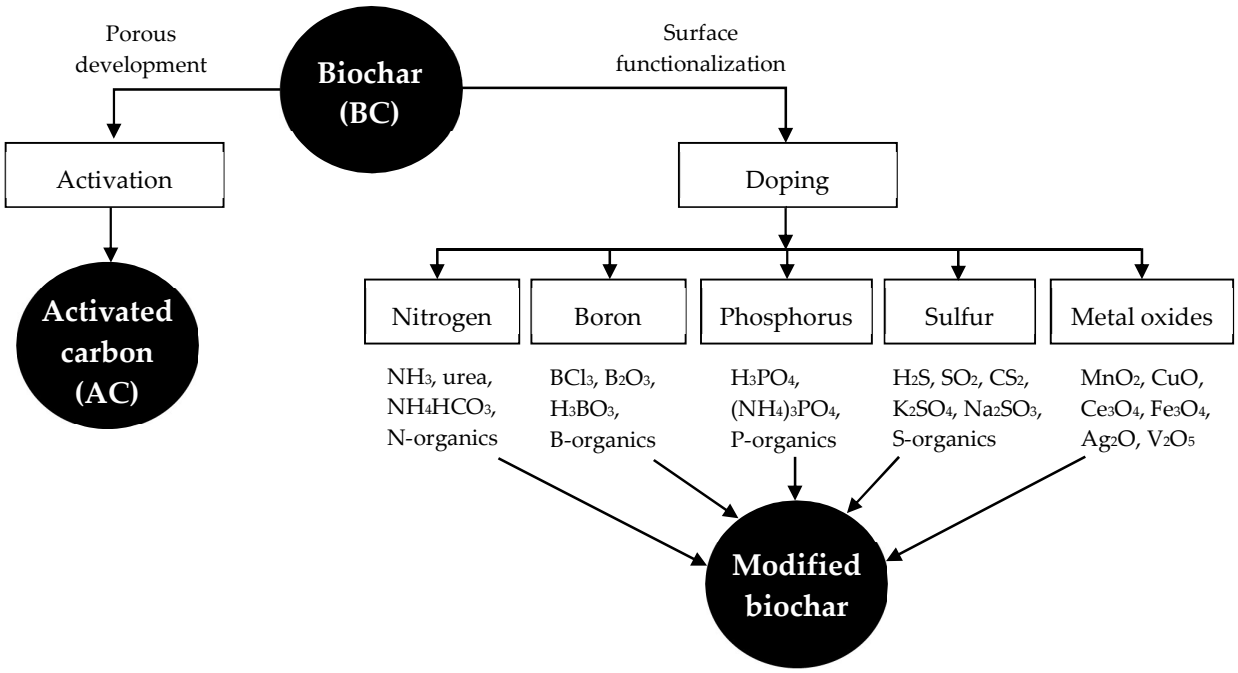

Figure 5. Biochar's modification processes to improve the adsorption capacities (Adapted from [67]).

3.2. Activated carbons

Activated carbon is an amorphous carbonaceous material with a very high porous development (total surface areas up to 3000 $m^2 \cdot g^{-1}$) that has a complex structure composed primarily of carbon atoms organized in disordered layers. There are two well-stablished procedures to synthesize activated carbon from biomass precursors, commonly known as physical and chemical activation (Figure 3). In the last decades the use of hydrothermal carbonization [78] and microwave heating [57] has been introduced as modifications of the traditional processes. Furthermore, the combination of chemical and physical activation is also considered to enhance the textural characteristics and generate more hierarchical porosity.

3.2.1. Physical activation

In physical activation, the biomass precursor is initially carbonized under inert atmosphere, and the resulting biochar is submitted to a partial and controlled gasification with steam, carbon dioxide, air/oxygen or a mixture of them. During the first step, carbonization, the starting material is transformed into fixed carbon with a low development of porous structure. The carbon yield is related to the biomass composition since carbonization removes the heteroatoms (non-carbon elements), which are volatilized at low temperature. In the second step, gasification selectively removes many of the reactive carbon atoms, generating the porosity and the final activated carbon structure. In case of CO_2 or H_2O activation, these reagents usually broaden the carbon porosity resulting in activated carbon with a wider porosity (meso- and macropores) especially at high burn-off values. The burn-off degree quantifies the mass removed during the gasification step, and can be calculated from:

$$\text{Burn off (\%)} = \frac{m_o - m_f}{m_o} \cdot 100, \quad (1)$$

where m_o is the initial mass (mass of biochar) and m_f is the mass after the gasification step or the mass of the final activated carbons. Generally, it is necessary to reach an equilibrium. Low burn-off values result in high carbon yields but low porosity development. In contrast, high burn-off degrees can produce activated carbon with high porous development (although extremely high burn-off values result in pore coalescence and, therefore, porosity reduction) but with low carbon yields. Gasification temperature is probably the synthesis parameter with the greatest effect on the properties of the final activated carbon. At low temperatures, the gasification reaction is chemically controlled, and narrow porosity is obtained. In contrast, when using high gasification temperatures, the gasification is controlled by the diffusion on the reagent through the structure of the biochar and wider pores are formed.

The main gasification reactions involving H_2O, CO_2 and O_2 as oxidizing reagents are shown below. In the case of oxygen, the gasification reaction is strongly exothermic, which forces a strict control of the reaction [79].

$$C + H_2O \rightarrow CO + H_2 \quad \Delta H_{25\,^oC} = +117\ kJ \cdot mol^{-1}, \quad (2)$$

$$C + CO_2 \rightarrow 2CO \quad \Delta H_{25\,^oC} = +159\ kJ \cdot mol^{-1}, \quad (3)$$

$$C + O_2 \rightarrow CO_2 \quad \Delta H_{25\,^oC} = -386\ kJ \cdot mol^{-1}, \quad (4)$$

$$2C + O_2 \rightarrow 2CO \quad \Delta H_{25\,^oC} = -256\ kJ \cdot mol^{-1}. \quad (5)$$

In order to reduce the cost of the activation process, some studies have synthesized activated carbons in a single thermal step, combining carbonization an activation in the presence of the activation reagent [80].

3.2.2. Chemical activation

Chemical activation usually begins with the impregnation step, in which the chemical activation agent is physically mixed with the biomass precursor. Chemical activation agents include a wide variety of salts, acids or bases, such as H_3PO_4 [81–83], H_2SO_4 [84,85], $ZnCl_2$ [86–89], $FeCl_3$ [54,90–94], NaOH [95–98] and KOH [95,99–101] among others. In this step, the most relevant variable is the impregnation ratio, i.e. the mass ratio between the chemical activating agent and precursor. The impregnation agent acts as dehydrating specie and inhibits the formation of tars, volatiles and other undesired products that can be formed during the carbonization stage. Due to this, it is affirmed that chemical activation processes result in higher carbon yields than physical activation ones. In the case of biomass precursors activated with strong bases (KOH and NaOH) can be necessary an initial carbonization step to avoid the direct oxidation of the biomass by the activating agent in the impregnation step. The biochar resulting from the carbonization step has a significantly higher fixed carbon content and can be subsequently impregnated with the activating agent. The precursor-activating agent mixture is next submitted to a thermal treatment at temperatures ranging from 400 to 1000 °C depending on the activating agent (see Figure 3) under inert atmosphere. In the last step the carbonized solid is washed to remove/recover the activating agent and free the porous structure of the final activated carbon. The main variables affecting the final porous structure of the activating carbon are the activating agent itself, the impregnation ratio and the activation temperature. Usually, strong bases (KOH and NaOH) yielded highly microporous activated carbons with high total surface areas, in some cases even higher than 3000 $m^2 \cdot g^{-1}$ [102]. In the case of the other activating agents the porosity could be tailored by the proper selection of the impregnation ratio and activating temperature. In general trend, the increase of the activation temperature results in higher porous development, although there is usually a maximum temperature from which the porous structure decreases. When it comes to the impregnation ratio (with values between 1:1 and 5:1), low impregnation ratios normally result in mainly microporous activated carbons, while high impregnation ratios produced a widening of the porosity, promoting formation of meso and macropores.

4. Characterization techniques

To understand the structure-adsorption relationships between the adsorption results and the adsorbent properties it is necessary to perform a complete characterization of the solid adsorbent. Two main characteristics of the adsorbent affect the adsorption process, namely the porosity and the amount of surface groups of the adsorbent. Therefore, the characterization of these properties is crucial for the understanding of the adsorption process and for the efficient design of new adsorbents with improved properties. A brief description of the techniques more usually used for the characterization of carbon adsorbent is explained below.

4.1. Textural charcaterization

The porous texture of carbon-based adsorbents can be characterized by physisorption techniques. Physisorption or physical adsorption occurs when a gas gets in contact with the solid surface of an adsorbent. The process is control by long-range Van der Walls dispersion forces and the short-range intermolecular repulsion [103]. The textural characteristics of the carbon adsorbents, including surface area and pore size distribution, are the main information obtained from physisorption characterization [104]. According to International Union of Pure and Applied Chemistry (IUPAC) pores can be classified in micropores (<2 nm), mesopores (2–50 nm) and macropores (>50 nm). The micropores can be further subdivided into ultramicropores (< 0.7 nm) and supermicropores (0.7-2 nm). During gas adsorption tests, the amount adsorbed, a, expressed per unit of mass of adsorbent depends on the adsorbate pressure, p, the adsorption temperature, T, and the adsorbent properties and gas–solid interactions [105]. The amount adsorbed can be expressed as: $a = f(P,T)$; and at a constant temperature: $a = f(P/P_o)$ being P_o the saturation pressure of the adsorbate at the temperature of measurement. This latter expression corresponds to the adsorption isotherm,

which represents the amount of gas adsorbed versus the pressure at constant temperature. IUPAC establish six different types of adsorption isotherms [106]. The solid sample should be heated under vacuum or purging gas prior to analysis to desorb the any adsorbed species from the surface. Outgassing under vacuum is especially relevant for the characterization of the porous structure of materials with very narrow micropores; where the adsorption can begin at very low relative pressures and therefore, requiring outgassing also down to very low pressures.

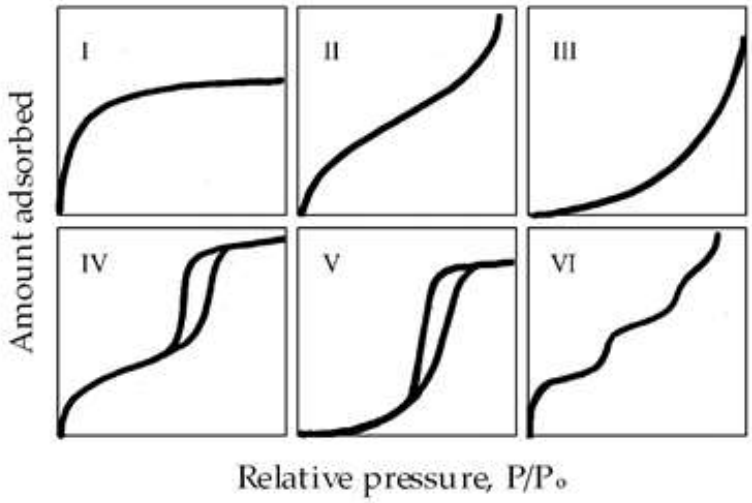

Figure 6. The IUPAC classification of adsorption isotherms.

N_2 adsorption-desorption at -196 ºC

Without doubt the technique more commonly used for the characterization of the textural structure of the adsorbents (including carbon-based ones) is N_2 adsorption-desorption at -196 ºC. The nitrogen adsorption mechanism begins with the micropore filling at low relative pressures ($p/p_o<0.4$). After that, mesopores are filled by capillary condensation with the consequent multilayer formation. In the mesoporous range ($p/p_o>0.4$), the desorption branch of the isotherm is not always superimposed to the adsorption one. This hysteresis phenomenon can be due to differences between rate of capillary emptying and filling, or to the interconnection of the mesopores blocked by filled micropores. Finally, at relative pressures close to 1, the filling of macropores is supposed to proceed also by multilayer formation. Different textural parameters can be determined from the N_2 adsorption-desorption isotherms, such as specific surface area, micropore and mesopore volume. Pores size distribution can also be calculated from this isotherm.

The *specific surface area* is probably the parameter that better characterizes the porosity of a solid and it represents the total surface of all the porosity. This area is calculated in the range of relative pressures from 0.01 to 0.3 approximately. The main method used for the calculation of the specific surface area is Brunauer–Emmett–Teller (BET) method [107]. The BET specific surface area is obtained from the cross-sectional area of a nitrogen molecule (0.162 nm^2) and supposing that the N_2 molecules are adsorbed on a continuous monolayer covering the entire adsorbent surface.

The *micropore volume and mesopore surface area* (also known as external surface area) are obtained from a reference sample similar to the porous studied material but non-porous. Two types of comparative plots are usually used, namely, the t-plot [108] and the α_s plot [109] that differ only in the reference solid adsorption isotherm presentation. The thickness of the surface film on the reference solid t is used to construct the t-plot. *Total pore volume* is usually calculated from the amount of N_2 adsorbed at relative pressures close to 1 (e.g.: $P/P_o = 0.99$) transformed to liquid phase. Finally, *pore size distribution* can be calculated from different approaches such as, Barrett-Joyner-Halenda (BJH) method [110], Horvath Kawazoe method [111] or density functional theory (DFT), among others.

CO_2 adsorption at 0 ºC

In the case of nitrogen adsorption at -196 ºC, the characterization of micropore smaller than 1 nm is very difficult since extremely low pressures are needed, with diffusion rates very slow and very long equilibration tines. In the view of this behavior, microporous materials should be characterized using other adsorbates such as carbon dioxide. Despite the kinetic diameters of N_2 (0.36 nm) and CO_2 (0.33 nm) are very similar, their adsorption is quite different mainly because their very different adsorption temperatures. At 0 ºC CO_2 is approximately 32 ºC below its critical temperature. Considering that its saturation pressure is very high (26,200 torr), the relative pressure necessary for the micropore filling are reached at moderate absolute pressures (1–760 torr) [112]. Therefore, CO_2 molecules can access the inner of ultramicropores despite the sizes of N_2 and CO_2 molecules are very similar. Furthermore, the equipment needed to carry out a micropore analysis with CO_2 is much simpler than those for argon or nitrogen adsorption. Since extremely low pressures are not required, turbomolecular pump and low-pressure transducers are not necessary. Because of these characteristics, CO_2 adsorption is considered a very useful tool for the characterization of the narrow microporosity.

4.2. Surface chemistry

The characterization of the surface chemistry is crucial for the complete understanding of the adsorbent-adsorbate interactions. The adsorption studies usually focused on the analysis of oxygen surface groups and the electrical charge density of the adsorbent's surface. Some of the more often used techniques are described below.

Fourier Transform Infrared (FTIR) Spectroscopy

Infrared (IR) spectroscopy consist of the quantification of the infrared radiation absorbed (or transmitted) by a material as a function of wavelength or frequency of the radiation. Since the absorption bands correspond to vibrations of a specific functional group of the molecule, band association allows the identification of the functional groups that constitute the material [113]. The FTIR spectrometers convert the infrared spectrum using Fourier transformation of the signal obtained with interferometer equipped with a moving mirror to produce. Numerical Fourier analysis allows to obtain a relationship between intensity and frequency, namely the FTIR spectrum [114]. FTIR measurements are usually performed with diluted carbon sample in KBr pellets in the wavelength range of 400 to 4000 cm^{-1}. Table 2 summarizes the assignment of FTIR absorption bands of biomass-derived carbons.

X-ray Photoelectron Spectroscopy (XPS)

XPS is performed by exciting the surface of a sample with mono-energetic Al Kα X-rays, which provokes the emission of photoelectrons from the sample surface. The energy of these emitted photoelectrons results in a photoelectron peak whose characteristic energy allows not only the identification of the corresponding element, but also the chemical state and amount of this element on the outermost layer (depth of approximately 5 nanometers) of the sample. Furthermore, the curve fitting of the XPS spectra allows the quantification of the surface atomic ratios. The deconvolution of the elemental spectra permits the analysis of the chemical bonding states and concentrations of the surface functional groups of carbon samples. Using this procedure, the C1s XPS spectrum can be deconvoluted into five different contributions as summarized in Table 3 [115]. It is well-known that heteroatoms, such as nitrogen and oxygen, can play a crucial role in the adsorption phenomena on carbon surfaces. Thus, it is important to analyze the type and amount of oxygen surface groups in order to determine the crucial surface properties such as hydrophobicity and surface polarity of the carbons. The O1s spectrum can also be fitted to three components (Table 3) [115]. In the case of the presence of nitrogen functionalities, the N1s spectra can also be deconvoluted and fitted considering pyridinic, pyrrolic and graphitic nitrogen atoms and nitrogen oxides. According to the area-simulating curve, the percentage of each component can be calculated.

Table 2. Assignment of FTIR absorption bands of biomass-derived carbons [116].

σ (cm^{-1})	Assignment	Designation
3700	υ (OH)	Free OH groups
3400	υ (OH)	Stretching in hydroxyl groups
2926	υ (C–H)	Stretching in alkyl groups
2870	υ (C–H)	Stretching in alkyl groups
1745	υ (C=O)	Stretching in aldehydes, ketones groups and esters
1642	υ (C=O)	Stretching in cyclic amide
1640	υ (C=C) υ (C=O)	Stretching in olefins carbonyl groups of carbon material highly conjugated in graphite layer
1552	υ (C=O)	Assigned to carbonyl groups conjugated in aromatic
1540	υ (C=C)	Assigned to skeletal stretch in condensed aromatic system
1520	υ (C=C)	Aromatic skeletal stretching bands
1462	υ (C-H)	Stretching in aromatic ring
1460	υ (C=O)	Stretching in cyclic amide
1444	υ (C=C), δ (CH)	Stretching in aromatic skeletal and ester
1150-1200	υ (C-O-C), υ (C-C),	Stretching vibration in pyranose ring skeletal or stretching in aromatic ring
1137	υ (C-O)	stretching in phenolic ring, carboxylic moiety
1069	υ (C-O-C)	Asymmetrical stretch vibrations
870, 690	γ (C-H)	Aromatic C–H out-of-plane bending vibrations
610	υ (O-H)	Stretching in OH groups
450	υ (C-C)	Stretching in C–C vibrations

Table 3. Assignment of C1s, O1s and N1s XPS peaks of biomass-derived carbons [115,117].

Elemental spectrum	Binding Energy (eV)	Assignation
C1s	284.1–284.4	C-C; C-H; graphite type
	284.8–285.2	C-OH; amorphous carbon, hydroxyl groups, phenolic, alcohol or ether aromatic carbon
	285.5–286.1	C-O-C; carbonyl groups
	286.3–287.6	O-C=O; carboxyl and ester groups
	289.5–290.0	π–π* transitions in the aromatic carbon
O1s	530.0–531.6	C=O
	532.7–533.3	C–OH or C–O–C
	534.8–535.7	chemisorbed oxygen
N1s	398.0–398.3	N-6 or pyridine-like structures
	400.0–400.3	N-5, i.e. pyrrolic
	401.1–401.6	graphitic nitrogen
	402.3–404.0	N-oxides

Temperature Programmed Desorption (TPD)

Temperature programmed desorption (TPD) coupled to mass spectroscopy (TPD-MS) can be used to determinate the nature of surface functional groups on carbons. Using this technique, gases produced from the decomposition of these groups are detected. The only gases evolved are carbon monoxide, carbon dioxide or water vapor and it is possible to recognize the presence of a functional group on the carbon surface considering its specific temperature of decomposition. Thus, surface oxygen-containing groups on carbon-based materials decompose upon heating in inert atmosphere yielding CO and CO_2 at different temperatures. TPD peaks can be assigned to the different oxygen functional groups by comparison with the results previously reported in the literature. Figure 7 represents the different surface oxygen groups on carbons and their approximate decomposition temperature in TPD tests. Water can be formed at high temperatures due to dehydration reactions of

Preprints (www.preprints.org) | NOT PEER-REVIEWED | Posted: 18 September 2018 doi:10.20944/preprints201809.0336.v1

Peer-reviewed version available at C 2018, 4, 63; doi:10.3390/c4040063

close carboxylic groups and phenol groups to anhydrides, lactones and ethers [118,119]. These groups then decompose upon heating to a mixture of CO and CO_2 at temperatures higher than 600 ºC.

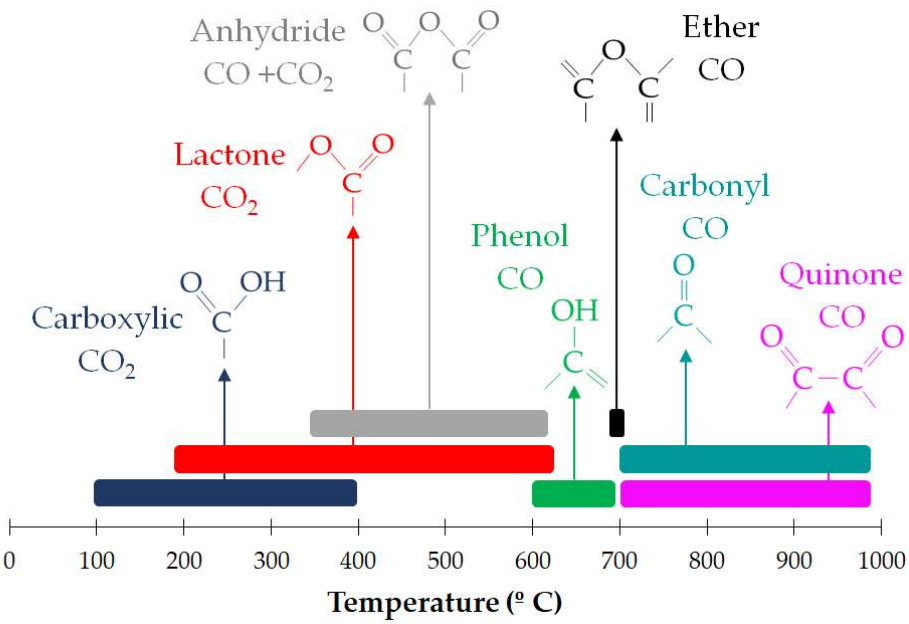

Figure 7. Surface oxygen groups on carbons and their approximate decomposition temperature by TPD test.

Boehm Tritation

The Boehm titration [120] is a simple technique developed for the quantification of acidic or basic functional groups on the surface of carbons. The method consists of a titration or selective neutralization of surface acidic groups of different strengths using bases that have conjugate acids covering a wide range of acid dissociation constants (Ka). The method is divided into two steps. In the first one, carbon materials get in contact with a reaction base that neutralize the more acidic oxygen groups on its surface. In the second step, the non-consumed amount of the base is determined by an acid–base titration. Therefore, Boehm tritation can be define as a reverse titration of the oxygen groups on the surface of the carbon [121]. For quantification of acidic groups, basic aqueous solutions—sodium hydroxide (NaOH), sodium carbonate (Na_2CO_3) or sodium bicarbonate ($NaHCO_3$)—are used. The consumed amount of $NaHCO_3$ (pKa = 6.37) is associated only to strong carboxylic acidity, whereas Na_2CO_3 (pKa = 10.25) reacts with lactonic and carboxylic oxygen surface groups, and NaOH (pKa = 15.74) with phenolic, carboxylic and lactonic acidic groups. For the characterization of weaker acidic groups, sodium ethoxide ($NaOC_2H_5$) is the other basic product used with absolute ethanol as solvent. However, sodium ethoxide is not often used because of the need to perform the experiment in non-aqueous media and under oxygen-free conditions. If the chosen concentrations of the used solutions decrease, the carbon dioxide effect can clearly appear on the titration curves. The relatively low concentration value of the reactant 0.01 $mol \cdot L^{-1}$ used allows determination of small amounts of functional surface groups with an interesting precision. Nevertheless, it also reveals clearly the carbon dioxide effect due to the presence of atmospheric CO_2, which dissolves in the solutions.

Point of zero charge

The point of zero charge (pH_{pzc}) can be defined as the pH at which the surface of an adsorbent is neutral, i.e., contains the same amount of positively charged surface functions than the negatively ones. In consequence, below this point of zero charge, the surface is positively charged; beyond this value, it is negatively charged. So in general terms, it is always easier to adsorb a cation on a negatively charged surface, and an anion on a positively charged surface. However, other

Peer-reviewed version available at C 2018, 4, 63; doi:10.3390/c4040063

interactions may be stronger than purely electrostatic forces, making the effect of surface charge not so important. Additionally, a cation is often complexed with ligands, some of them being possibly negatively charged. Therefore, in such a case, the cation is in fact a negative complex, which may adsorb very well on a positively charged surface. The determination using the pH drift method is very simple, 50cm^3 of 0.01M NaCl solution was placed in a closed Erlenmeyer flask. The pH was adjusted to a value between 2 and 12 by adding HCl 0.1M or NaOH 0.1M solutions. Then, 0.15 g of each AC sample was added to each flask. After 48 h under agitation at room temperature the final pH is measured. The point of zero charge is the point where the curve pH_{final} vs. pH_{inital} crosses the line $pH_{initial}$=pH_{final} [122,123].

5. Experimental procedures for adsorption tests

Adsorption can be defined as an enrichment of chemical compounds from a fluid on the surface of a solid material. In the case of water treatment or purification, this process can remove efficiently a wide variety of solutes. Solid surfaces are energetically heterogeneous, i.e., they contain energy-rich sites with different energies that are able to interact with solutes. In adsorption, the solid material is referred as adsorbent; and the species adsorbed are denoted as adsorbate. The modification of some properties of the liquid phase, such as temperature, pH or concentration of adsorbate, can result in the desorption of the adsorbed species from the surface into the liquid phase [124].

The amount adsorbed, q, is usually defined as the number of moles or mass adsorbed per adsorbent mass. In practical application adsorption theory can be studied in three different approaches: the adsorption equilibrium, the adsorption kinetics, and the adsorption dynamics. The adsorption equilibrium analyzed the effect of adsorbate concentration and adsorption temperature on the adsorbed amount. Usually, the adsorption equilibrium is considered at a fixed temperature and expressed in the form of the adsorption isotherm:

$$q = f(C); \qquad T = \text{constant}, \tag{6}$$

where C represents the adsorbate concentration in the liquid phase.

The adsorption kinetics studies the evolution of the adsorbed amount with the time also at a constant temperature.

$$q = f(t); \qquad T = \text{constant}, \tag{7}$$

where t is time. Slow mass transfer processes from the liquid to the solid phase generally control the adsorption rate.

Finally, in practical applications, adsorption is performed in fixed-bed adsorbers, in which adsorption depends not only on time but also on the location inside the bed. The dependence on time (t) and space (z) is referred as column dynamics or adsorption dynamics.

$$q = f(t,z), \qquad T = \text{constant}. \tag{8}$$

The adsorption equilibrium constitutes the foundations of all adsorption approaches, being its study necessary for the proper understanding of both adsorption models, kinetic and dynamic. To forecast the behavior of adsorption dynamics, the analysis of adsorption equilibrium and kinetics is indispensable [124].

5.1. Adsorption equilibrium

The determination of equilibrium data is crucial to understand the adsorption processes, to characterize the tendency to adsorb of different water pollutants, to choose the most favorable adsorbent, and to design batch and fixed-bed adsorption reactors. The adsorption equilibrium is strongly affected by the characteristics of the adsorbate-adsorbent couple but also by the pH and temperature of the liquid phase, and the existence of competing adsorption.

Typically, the adsorption equilibrium is obtained experimentally at constant temperature, and the experimental points are fitted by a mathematical equation that constitutes the isotherm equation. To obtain equilibrium data, and the subsequent isotherm equation, the bottle-point method is the more often used. In this procedure, different isotherm points are calculated by using different bottles in parallel (a minimum number of approximately 8 bottles is advisable to get enough data points). Each bottle is filled with a specific volume of adsorbate solution, V, with an initial concentration, C_o. Afterwards a mass of the adsorbent, m, is added to each bottle under shaking or stirring until equilibrium state is achieved. One of the problems of this methodology is to assure enough contact time to reach the adsorption equilibrium, which could vary between a few hours and several days. It is worth mentioning the strong influence of the adsorbent particle size in equilibrium time, with longer equilibrium times for larger particles sizes due to the increasing diffusional effects. The equilibrium time could be estimated from the kinetic tests described in the following chapter. Once equilibrium is achieved, the equilibrium concentration of the adsorbate in the liquid phase, C_e, has to be quantified. Then, the specific adsorbed amount, q_e, is determined from the material balance equation:

$$q_e = \frac{(C_o - C_e)\,V}{m}\,. \tag{9}$$

Up to the date, there is no isotherm equation describing properly all experimental isotherm curves. In contrast, many isotherm equations have been obtained from theoretical or empirical models. Although, the objective should be finding an isotherm model as simply as possible to be used for adsorber design. Probably, the most used adsorption isotherms are those proposed by Langmuir [125] and Freundlich [126]. The *Langmuir isotherm* has the form:

$$q = \frac{q_m b C}{1 + bC}, \tag{10}$$

where q_m and b are the isotherm parameters. The parameter q_m has the same unit as the adsorbent loading (usually, $mg \cdot g^{-1}$ or $mmol \cdot g^{-1}$), and the unit of b is the reciprocal of the adsorbate concentration unit. Langmuir model supposes that adsorption proceeds through a monolayer coverage of the adsorbent surface with energetic homogeneity of the adsorption sites. Obviously, this assumption is not fulfilled for all the pairs adsorbent-adsorbate, resulting in an inadequate adjustment of the experimental results. Langmuir isotherm model could be linearized to avoid more complicated non-linear regression. Different linearizations are possible:

$$\frac{C}{q} = \frac{1}{q_m b} + \frac{1}{q_m} C, \tag{11}$$

$$\frac{1}{q} = \frac{1}{q_m} + \frac{1}{q_m b}\frac{1}{C}, \tag{12}$$

$$q = q_m - \frac{1}{b}\frac{q}{C}, \tag{13}$$

$$\frac{q}{C} = q_m b - qb. \tag{14}$$

As an alternative, *Freundlich isotherm* can be used:

$$q = KC^n, \tag{15}$$

being K and n the characteristic parameters of the Freundlich isotherm. K is known as the adsorption coefficient and it is related to the strength of adsorption. High K values correspond with higher is the

amounts of adsorbent loading. The exponent n is related to the curvature of the isotherm and reflects the energetic heterogeneity of the adsorbent surface. Values of n lower than 1 yield concave isotherms, an n value equal to 1 result in a liner isotherm and if n is higher than 1 the isotherm is convex (Figure 8). Many of the studies in the literature reported n values lower than 1, with high adsorbed amounts at low concentrations. Due to this, these isotherms are considered as favorable isotherms, while isotherms with n > 1 are defined as unfavorable. The unit of K (= q/C^n) depends on the units used for q and C and includes the exponent n. The conversion of these K units from one study to another for comparison purposes is not straightforward due to the included exponent n. Tables for K unit conversions could be found elsewhere [124]. Freundlich isotherm could be also linearized as follows:

$$\ln q = \ln K + n \ln C, \tag{16}$$

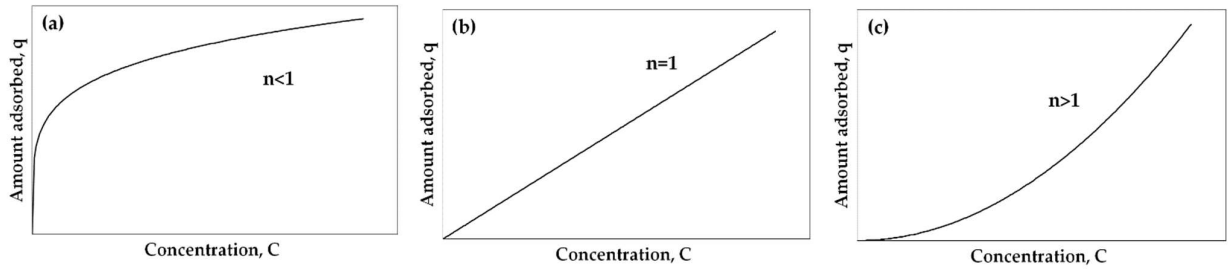

Figure 8. Forms of the Freundlich isotherm depending on the n value: (a) n < 1, (b) n = 1, and (c) n > 1.

Adsorption equilibrium results are also fitted by Dubinin-Radushkevich (DR) model, which is developed from the theory of volume filling of micropores (TVFM) [127]. The mathematical expression of this isotherm is shown below:

$$q = \frac{V_p}{V_m} \exp\left[-\left(\frac{RT \ln \frac{C_{sat}}{C}}{E_c}\right)^2\right], \tag{17}$$

where R is the universal gas constant, T is the adsorption temperature, C_{sat} is the saturation concentration of the adsorbate and V_m is the molar volume of the adsorbate. The isotherms parameters are V_P, the specific pore volume, and E_C, the characteristic adsorption energy. In this isotherm model, q is the molar loading expressed in adsorbate moles per gram of adsorbent V_P and V_m units are $cm^3 \cdot g^{-1}$ and $cm^3 \cdot mol^{-1}$, respectively. The term $RT\ln(C_{sat}/C)$ is known as adsorption potential, ε.

$$\varepsilon = RT \ln \frac{C_{sat}}{C}. \tag{18}$$

The linearization of the Dubinin-Radushkevich (DR) model is shown below:

$$\ln q = \ln \frac{V_p}{V_m} - \frac{1}{E_C^2}\left(RT\ln \frac{C_{sat}}{C}\right)^2. \tag{19}$$

Two parameters isotherms, such as those previously mentioned, cannot properly describe adsorption results over a broad concentration range. In those cases, different isotherm parameters should be specified for narrower concentration ranges or three-parameter isotherms should be used. Table 4 summarizes the characteristic equations of isotherms with three parameters. Isotherm model with more than three parameters are hardly ever used.

Table 4. Characteristic equations of isotherm models with three parameters.

Model	Equation	
Langmuir-Freundlich isotherm/Sips isotherm	$q = \frac{q_m (bc)^n}{1 + (bc)^n}$	[128]
Redlich-Peterson isotherm	$q = \frac{q_m bc}{1 + (bc)^n}$	[129]
Tóth isotherm	$q = \frac{q_m bc}{[1 + (bc)^n]^{1/n}}$	[130]
Dubinin-Astakhov (DA) equation	$q = \frac{V_p}{V_m} \exp\left[-\left(\frac{RT \ln \frac{C_{sat}}{C}}{E_c}\right)^m\right]$	[131]

5.2. Adsorption kinetics

Any adsorption process, especially those performed on porous adsorbents requires a time to achieve the equilibrium state due to the existence of mass transfer resistances. The evolution of the amount adsorbed with time is known as adsorption kinetics. Diffusion through the particle external surface and inner porosity controls the rate of adsorption. The determination of the mass transfer parameters as well as a proper equilibrium model are necessary for the design of adsorber reactors, slurry or fixed-bed.

The adsorption process proceeds by four successive steps: (i) diffusion of the adsorbate from the liquid phase to the hydrodynamic boundary layer surrounding the adsorbent particle, (ii) diffusion through this layer to the external surface of the adsorbent (film diffusion or external diffusion), (iii) diffusion through the inner porosity of the adsorbent particles (intraparticle diffusion or internal diffusion), and (iv) energetic interaction between the adsorbate and the adsorption sites. Usually the first and the fourth steps are supposed to happen very fast. Therefore, the slower step between film and intraparticle diffusion determines the global adsorption rate. To clarify what step controls the adsorption rate, it should be considered that film diffusion depends on the hydrodynamic conditions. Therefore, if an increase of the stirrer velocity (slurry adsorbers) of the flow velocity (fixed-bed adsorbers) result in an increase of the adsorption rate, the kinetics of the process is controlled by film diffusion. In contrast, the adsorbent particle size affects both the film diffusion and the intraparticle diffusion as a consequence of changes of surface area and diffusion paths, respectively. The intraparticle or internal diffusion mechanisms happen by effective pore volume diffusion, surface diffusion, or a combination of both mechanisms. The effective pore volume diffusion can be defined as the movement of the adsorbate molecules through the inner porosity of the adsorbent particles and it is denoted by D_P, the effective pore volume diffusion coefficient. On the other hand, the surface diffusion is related to the transport of the adsorbate on the surface of the adsorbent particles, from higher energy sites to lower energy sites. This mechanism is represented by the surface diffusion coefficient, denoted as D_S [132].

Adsorption kinetic curves, C = f(t), are obtained by following the change of the concentration of the adsorbate with time in a specific solution volume (V) with a known mass of adsorbent (m). The fitting of the kinetic curve to the different adsorption kinetic models allows the determination of the mass transfer coefficients. The mass transfer coefficients of film diffusion determined experimentally depend on hydrodynamic conditions and, therefore, they cannot be used in other experimental conditions. Due to this, most kinetic tests focus exclusively on internal diffusion, which is not affected by hydrodynamic conditions. Consequently, the conditions of the kinetic tests are chosen to obtain very fast film diffusion in order to avoid considering this step in kinetic model. To avoid the influence of film diffusion a minimum stirrer or flow velocity, for slurry or fixed-bed adsorbers, respectively, should be used. This minimum velocity can be estimated obtaining different kinetic curves with increasing stirrer or flow velocities up to invariable kinetic curves.

Probably the most complete diffusional model is the *pore volume and surface diffusion model (PVSDM)*. This model assumes constant adsorption temperature; spherical adsorbent particles, and negligible transport by convection inside the pores. The intraparticle diffusion can happen by pore volume diffusion mechanism and surface diffusion mechanism or both. The values of effective pore

volume diffusion coefficient (D_P) and effective surface diffusion coefficient (D_s) are considered constant and the adsorption rate on an active site instantaneous [132,133]. This model is described by the following equations:

$$V\frac{dC_t}{dt} = -mSk_F\left(C_t - C_{s(t)}|_{r=R}\right), \quad (20)$$

$$t = 0;\ C_t = C_0, \quad (21)$$

$$\varepsilon_p\frac{\partial C_r}{\partial t} + \varrho\frac{\partial q}{\partial t} = \frac{1}{r^2}\frac{\partial}{\partial r}\left[r^2\left(D_p\frac{\partial C_r}{\partial r} + \varrho_p D_s\frac{\partial q}{\partial r}\right)\right], \quad (22)$$

$$t = 0;\ 0 \le r \le R;\ C_r = 0, \quad (23)$$

$$\frac{\partial C_r}{\partial r}|_{r=0} = 0, \quad (24)$$

$$D_p\frac{\partial C_r}{\partial r}|_{r=R} + \varrho_p D_s\frac{\partial q}{\partial r}|_{r=R} = k_F\left(C_t - C_{s(t)}|_{r=R}\right), \quad (25)$$

where V is the solution volume, m is the adsorbent mass, S is the external surface area per mass of the adsorbent, k_F is the external mass transfer coefficient, R is radius of the adsorbent particles, ε_P is the void fraction of the adsorbent, ϱ_P is the apparent density of the adsorbent, C_0 is the initial adsorbate concentration in the bulk solution, C_r is the adsorbate concentration varying with the position and time, and q is the mass of adsorbate per mass of adsorbent varying with the position and time, respectively. The PVSDM model can be simplified by considering that the sole intraparticle diffusion mechanism may be either *pore volume diffusion (PVDM)* ($D_S = 0$) or *homogeneous surface diffusion (HSDM)* ($D_P = 0$). The solution of this model assumes that exists a local equilibrium between the adsorbate concentration of the pore solution, Cr, and the mass of adsorbate adsorbed on the pore surface, q, represented by the adsorption isotherm [132].

Although diffusion models are appropriate to describe adsorption kinetics for porous adsorbents, the complexity of the solution of the equations that describe this model has resulted in an increasing number of studies describing the adsorption kinetics by more simple models based on chemical reaction kinetics. These adsorption reaction models describe adsorption as a single phenomenon, unlike diffusive models. The most analyzed models are the pseudo-first-order and pseudo second-order models, and Elovich equation [134].

The *pseudo-first order model* is described by the equation:

$$\frac{dq_t}{dt} = k_1\left(q_e - q_t\right), \quad (26)$$

where q_e and q_t ($mg{\cdot}g^{-1}$) are the adsorption capacities at equilibrium and time t (min), respectively, and k_1 (min^{-1}) is the pseudo-first-order rate constant of the kinetic model. The solution of this equation with the initial condition $t = 0$; $q = 0$ and $t = t$; $q = q_t$ results in:

$$\ln\left(\frac{q_e}{q_e - q_t}\right) = k_1{\cdot}t \qquad \text{or} \qquad q_t = q_e{\cdot}[1 - \exp(k_1{\cdot}t)], \quad (27)$$

Different studies about the adsorption of pollutants from liquid phase confirm this model as the most appropriate to represent adsorption kinetics.

The *pseudo-second order model* [135] can be expressed by:

$$\frac{dq_t}{dt} = k_1\left(q_e - q_t\right)^2, \quad (28)$$

where k_2 is the pseudo-second order rate constant with units $g \cdot mg^{-1} \cdot min^{-1}$. The integration of the above equation with the initial condition of $q_t = 0$ at $t = 0$ and $q_t = q_t$ at $t = t$, yields:

$$\frac{1}{(q_e - q_t)} = \frac{1}{q_e} + k_2 \cdot t, \tag{29}$$

or alternatively:

$$q_t = \frac{t}{\left(\frac{1}{h_0}\right) + \left(\frac{t}{q_e}\right)} \quad ; \quad h_0 = k_2 \cdot q_e^2, \tag{30}$$

where h_0 ($mg \cdot g^{-1} \cdot min^{-1}$) is the initial adsorption rate. This model has been also successfully applied to the adsorption of different compounds from aqueous solutions.

Finally, the *Elovich model* [136] was described by the next differential equation:

$$\frac{dq}{dt} = \alpha e^{-\beta q}, \tag{31}$$

where α ($mg \cdot min^{-1} \cdot g^{-1}$) is a constant associated to chemisorption rate and β ($g \cdot mg^{-1}$) is a constant related to the extent of surface coverage. Assuming that $\alpha\beta t >> 1$, and with the initial condition of $q = 0$ at $t = 0$ and $q = q$ at $t = t$, this equation can be solved in:

$$q_t = \beta \ln(\alpha\beta) + \beta \ln(t). \tag{32}$$

β can be directly obtained from the slope of the plot of $q \cdot t$ versus $\ln(t)$. And α can be calculated from the intercept of the same plot once β is known.

5.3. Adsorption dynamics

Many real adsorption procedures proceed in continuous operation conditions in fixed bed adsorbers [137,138]. In this type of adsorbers, the stream goes through a column packed with the adsorbent particles and the pollutants are continuously adsorbed during the operation until exhaustion of the adsorbent capacity. Breakthrough curves consist of the representation of the outlet concentration as a function of the adsorption time up to saturation of the adsorber, i.e. equal inlet and outlet concentrations. Figure 9 shows the typical breakthrough curve, representing the evolution of the outlet concentration with adsorption time. The concentration increases due to the limited adsorption capacity of the bed. The zone represented in grey color is the mass transfer zone, defined as the part of the adsorbent bed where adsorption is happening and therefore, the concentration varies in the direction of the flow. Breakthrough happens when the leading forward part of this zone reaches the exit of the column. The breakthrough concentration C_b is defined as the maximum concentration allowed at the outlet stream and it depends strongly on the requirements that the outlet stream need to fulfill.

In the mathematical modeling of fixed-bed adsorption processes, some assumptions must be adopted: (i) the system behave as isothermal, without temperature variations through the bed produced by the adsorption process itself; (ii) only one adsorbate is present in the liquid stream; (iii) the concentration of the solute in the liquid is small, so that adsorption does not produce any change the liquid flow rate; (iv) there is not radial velocity and therefore; (v) the adsorbate concentration in both phases in the radial directions are constant [132]. Assuming these suppositions, the mass balance equation of the column can be expressed as:

$$\frac{\partial C}{\partial t} + v\frac{\partial C}{\partial z} + \frac{1-\varepsilon}{\varepsilon}\varrho_p\frac{\partial q}{\partial t} = D_L\frac{\partial^2 C}{\partial z^2}, \quad (33)$$

where v is the flow liquid velocity (cm·s^{-1}), ϱ_p is the adsorbent particle density (g·cm^{-3}), D_L is the axial dispersion coefficient (cm^2·s^{-1}), and z is the spatial coordinate for the column length (cm). The adsorption rate, ∂q/∂t, can de described by one of the kinetic models defined in the previous section. This equation can be numerically solved using the following initial and boundary conditions:

$$t = 0;\ C = 0;\ q = 0, \quad (34)$$

$$t > 0;\ z = 0;\ q = 0, \quad (35)$$

$$t \to \infty;\ \frac{\partial C_i}{\partial t} = 0;\ \frac{\partial q}{\partial t} = 0. \quad (36)$$

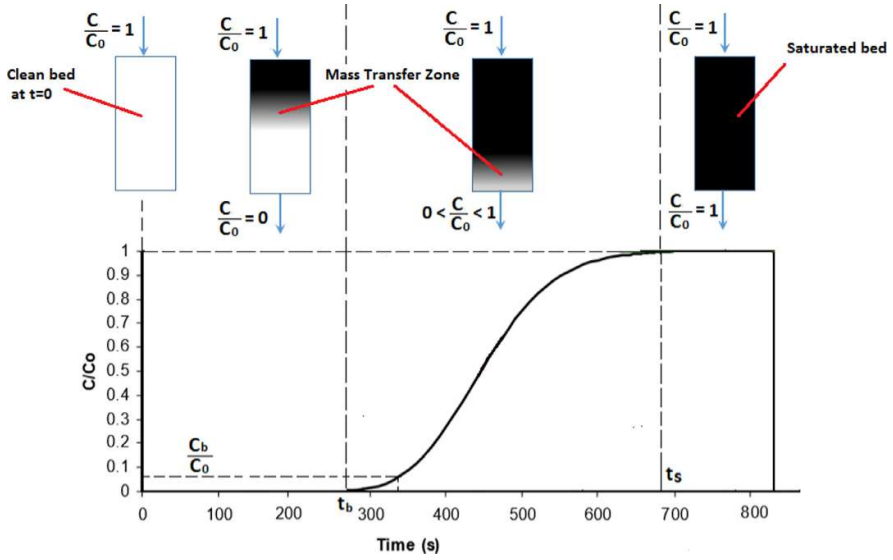

Figure 9. Typical breakthrough curve (C_b = breakthrough concentration; C_o =feed concentration; t_b = breakthrough time; t_s = saturation time) (Reprinted from [139] with permission from Elsevier).

Different numerical methods have been explored to estimate the mass balance equation for fixed-bed adsorbers. However, the use of this rigorous model requires the knowledge of many interdependent kinetic parameters before solution [140]. Due to this, empirical models with high accuracy but significant less parameters has been proposed in the literature [141]. Some of them are briefly described in the following lines.

The *Bohart-Adams model* [142] was obtained applying the surface reaction theory that considers that the equilibrium is not reached instantaneously, and adsorption rate is proportional to both the adsorption capacity and the concentration of solute in the liquid. This model is very suitable for adsorption processes with high affinity equilibrium behavior (or irreversible isotherm) [132,143]. The linearized expression of the Bohart–Adams equation is:

$$\ln\left(\frac{C_0}{C} - 1\right) = \frac{k_{BA}N_0 z}{u} - k_{BA}C_0 t, \quad (37)$$

where k_{BA} is the Bohart–Adams rate constant (cm^3·mg^{-1}·min^{-1}), N_0 is the adsorption capacity per unit volume of sorbent bed (mg·cm^{-3}), z is the bend length (cm), and u the superficial velocity (cm·min^{-1}).

Plotting $\ln[(C_0/C) -1)]$ versus t gives a straight line whose slope is $-k_{BA}C_0$ and the intercept with the Y-axis is equal to $k_{BA}N_0z/u$.

The Thomas model [144] assumes Langmuir adsorption isotherms, kinetic following a pseudo-second-order model and no axial dispersion. Under these conditions, the linearized solution of the mass balance equation could be expressed as:

$$\ln\left(\frac{C_0}{C} - 1\right) = \frac{k_T q_0 m}{Q} - k_T C_0 t, \quad (38)$$

where k_T is the Thomas rate constant ($cm^3 \cdot mg^{-1} \cdot min^{-1}$), q_0 is the saturation adsorption capacity ($mg \cdot g^{-1}$), m is the adsorbent mass in the column (g) and Q is the operating flow rate ($cm^3 \cdot min^{-1}$).

The *Yoon-Nelson model* [145] was proposed to predict the breakthrough curves of gas-phase adsorbates on activated charcoal. This model supposes that the rate of adsorption is proportional to the adsorption rate and the yield curve of the adsorbed material. The linearized equation of the Yoon-Nelson model can be expressed as:

$$\ln\left(\frac{C}{C_0 - C}\right) = k_{YN}(t - \tau), \quad (39)$$

where k_{YN} is the rate constant (min^{-1}), and τ is the time (min) required for 50% adsorbate breakthrough. Both parameters can be obtained from the plot of a $\ln[C/(C_0-C)]$ versus t. This model does not require any information about the adsorbent particles and/or bed properties.

Finally, the *Wolborska model* [146] was proposed to predict the breakthrough plots at low concentration of the adsorbate. The linearized expression of the Wolborska model corresponds to:

$$\ln\left(\frac{C}{C_0}\right) = \frac{\beta_a C_0}{N_0} t - \frac{\beta_a z}{u}, \quad (40)$$

where C_0 is the inlet concentration of adsorbate ($mg \cdot l^{-1}$), β_a is a kinetic coefficient for external mass transfer (min^{-1}), N_0 is the maximum amount adsorbed per unit volume of adsorbent ($mg \cdot l^{-1}$), Z is the bend length (cm), and u is the superficial velocity ($cm \cdot min^{-1}$). From the plot of $\ln(C/C_0)$ versus t, β_a can be calculated from the intercept with the Y axis, and N_0 from the slope once β_a is determined. In some studies it is observed that this model fits properly only to the initial part of the breakthrough plot [147]. More empirical models for the fitting of the breakthrough adsorption curves could be found elsewhere [139].

6. Adsorption of emerging contaminants on biomass-derived carbons

6.1. Adsorption on biochars

This section summarizes the results about adsorption of emerging contaminants on biochars or modified-biochar. The literature contains numerous references about activated biochars which are intentionally omitted in this section, since an activated biochar can be considered an as activated carbon and therefore included in the following section focused on adsorption on activated carbons.

Antibiotics are frequently detected in water streams due to its widespread use by today's society. Among them, various sulfonamides, based on SO_2NH_2 group, are used regularly because of their antibacterial activity. Among them sulfamethoxazole (SMX) has been chosen as target pollutant in many reported works. It was adsorbed at different pH on magnetic biochar derived from pine sawdust [148]. The amount adsorbed decreases with increasing pH values, especially at the highest pH analyzed (8.5). The authors conclude that the adsorption mechanism is controlled by π-π electron donor acceptor and hydrophobic interactions. The adsorption of sulfamethoxazole on a biochar from pelletized pine-forestry waste and the subsequent thermal regeneration in fixed-bed adsorber was also analyzed [149]. It was observed a more than 3-fold augment of the adsorption capacity of sulfamethoxazole after thermal regeneration of the adsorbent bed. Zheng et al. [150] analyzed the

adsorption of SMX on *Arundo donax* derived biochars carbonized at different temperatures in the range of 300 to 600 ºC and different pH values. Authors report that neutral SMX molecules (SMX^0) were dominant for sorption at pH 1.0-6.0, while above pH 7.0, although biochars surfaces were negatively-charged, anionic SMX species sorption increased with pH and is regulated via charge-assisted H-bonds. The SMX^0 sorption at pH 5.0 was nonlinear and was controlled for all biochars via hydrophobic interaction, π-π electron donor-acceptor interaction and pore-filling. Regarding the temperature used to carbonize the biochars, it was described that the removal of inorganic fraction by low-temperature biochars (e.g., 300 ºC) reduced SMX sorption, while enhanced the sorption by high-temperature biochars (e.g., 600 ºC) due to the presence of temperature-dependent inorganic fractions in the biochars. Xie et al. [151] analyzed the adsorption of sulfamethoxazole and sulfapyridine on three pine-wood biochars. For both sulfonamides, the adsorbent surface area-normalized adsorption was stronger at higher pyrolysis temperature, probably due to the enhanced π-π electron-donor-acceptor interaction with the carbon surface by the higher degree of graphitization. Despite the relatively large difference in surface O-functionality content between the biochars, their surface area-normalized adsorption was very similar, suggesting a low-significant role of the surface O-functionalities. The simultaneous removal of cadmium (Cd) and SMX on rice straw biochar were investigated by Han et al. [152]. Equilibrium results were well described by the Langmuir isotherm. The maximum adsorption capacity of SMX increased notable in the presence of Cd (from 1.83 up to 9.18 $mg \cdot g^{-1}$) probably as a consequence of the formation of surface complexes between Cd or SMX and carboxyl or hydroxyl groups. Ahmed et al. [153] reported both the single and competitive sorption of several sulfonamides, namely, sulfamethazine, sulfamethoxazole and sulfathiazole on functionalized biochar. The experimental equilibrium data followed well Langmuir and Freundlich models for single solutes, and by the Langmuir model for competitive solutes. The adsorption capacities were in the order sulfathiazole >sulfamethoxazole>sulfamethazine, with about three times lower adsorption capacities in competitive than in the single adsorption. The kinetic data were best described by the pseudo second-order (PSO) model for single solutes, and by PSO and intra-particle diffusion models for competitive solutes. Adsorption mechanism was governed by pore filling through diffusion process. The adsorption of neutral species seems to proceed by strong H-bonds followed by π-π electron-donor-acceptor, and by Lewis acid-base interaction. In contrast, the adsorption of positive sulfonamides species is mainly due to π-π electron-donor-acceptor interactions. Finally, in the case of the sorption of negative species was controlled by proton exchange, although with a significant role of π-π electron-acceptor-acceptor interactions. Li et al. [154] investigated the sorption of SMX on biochars derived from rice straw (RS) and alligator flag (AF). The adsorption was well described by the Langmuir isotherm with maximum adsorption capacities of 3.65 $mg \cdot g^{-1}$ with rice straw derived adsorbent. The presence of Cu^{2+} and/or Cd^{2+} ions at relatively low concentrations (20 $mg \cdot L^{-1}$) significantly enhanced the adsorption capacity.

Other important antibiotic presents in urban wastewater is the tetracycline, a broad-spectrum antibiotic usually used in treatments of various infections. Rice husk derived biochar was used for the adsorption of this antibiotic [155]. The biochar was modified by simple acid and alkali treatments. It was concluded that the alkali treatment increased the adsorption capacity of tetracycline probably as a consequence of the higher development of surface area. Jing et al. [156] analyzed the enhanced adsorption of tetracycline on methanol-modified biochar from rice husk. The modified biochar showed not only a higher capacity of tetracycline adsorption (both in batch and continuous adsorption tests), but also a faster adsorption kinetic, probably because of the increase in the amount of surface oxygen groups in the modified biochar. Recently, Chen et al. [157] reported tetracycline adsorption capacities up to 167.5 $mg \cdot g^{-1}$ using H_3PO_4-modified biochars from pig manure and rice straw. The adsorption mechanism seems to proceed through H-bonding and π-π electron donor acceptor interactions, which can explain the increase of the adsorption with pH increasing from 5.0 to 9.0. Even higher tetracycline adsorption capacities were reported when using alkali-acid modified biochar with magnetic properties obtained from sewage sludge [158]. According to density functional theory model calculations, the adsorption mechanism was controlled by strong π-π stacking interaction and pore-filling effect. Wang et al. [159] reported the sorption of tetracycline from aqueous

solution on biochars synthesized by pyrolysis at 300, 500 and 700 ºC of rice straw. Both the Freundlich and Langmuir isotherms describe properly the experimental adsorption data, with an increase in the adsorption capacity with increasing pyrolysis temperature (maximum capacity of 14.16 $mg \cdot g^{-1}$ at 25 ºC). The relatively high surface area (28 $m^2 \cdot g^{-1}$) of the biochar pyrolyzed at the highest temperature and the π–π electron-donor acceptor contributed to this high adsorption capacity. A thermodynamic analysis indicated that the tetracycline adsorption process was spontaneous and endothermic.

Female hormones, such as 17β-estradiol, used in various medical treatments have also been detected in residual urban waters. The effect of the pyrolysis temperature on the adsorption of 17β-estradiol on rice straw-derived biochar was analyzed elsewhere [160]. The adsorption mechanism was governed by electrostatic attractions and π-π interaction. The chars synthesized at higher carbonization temperatures showed higher adsorption capacities than those corresponding to the biochars obtained at lower carbonization temperatures. The maximum adsorption capacity obtained by fitting of the experimental data to Langmuir model isotherm was almost 65 $mg \cdot g^{-1}$. Dong et al. [161] analyzed the adsorption of 17β-estradiol using highly adsorptive magnetic biochar nanoparticles from bagasse. The adsorption kinetics were described by a pseudo-second-order model with a maximum adsorption capacity of 50.2 $mg \cdot g^{-1}$. FTIR analyses suggested that adsorption proceeds through simultaneous hydrophobic interactions and π–π electron donor-acceptor interactions, while the controlling mechanism can change from hydrophobic to π–π interactions with increasing pyrolysis temperature.

Essandoh et al. [162] analyzed the adsorption of salicylic acid and ibuprofen from aqueous solutions on pine wood biochar. Adsorption kinetics followed pseudo-second order model for both adsorbates. The adsorption capacities obtained from Langmuir model were 22.70 and 10.74 $mg \cdot g^{-1}$ for salicylic acid and ibuprofen, respectively, despite the low porosity of the pinewood biochar (1.35 $m^2 \cdot g^{-1}$). A strong influence of the pH on the amounts adsorbed was observed. Salem and Yakoot [163] reported ibuprofen adsorption capacities of approximately 170 $mg \cdot g^{-1}$ and adsorption kinetics following a pseudo-second order model on rice straw based biochar carbonized at different temperatures. The authors also conclude that ibuprofen adsorption happens by π-π interactions.

Lonappan et al. [164] reported the adsorption of diclofenac, a nonsteroidal anti-inflammatory drug, on biochars derived from pine wood and pig manure. It was stated that diclofenac adsorption on pine chars was strongly affected by pH. However, the adsorption on pig manure derived biochar is not so affected by the pH variations, probably as a consequence of the higher amount of surface functional groups of pig manure biochar as well as the diclofenac hydrophobicity.

Tong et al. [165] reported the adsorption of triclosan, an antimicrobial used for personal hygiene and disinfection products, on acid treated biochar pyrolyzed at different temperatures in the range of 300 to 800 ºC. The maximum triclosan uptake, 0.87 $mg \cdot g^{-1}$, was obtained with the biochar obtained at 800 ºC. The biochar adsorbent show little variation in its adsorption capacities at pH between 5 and 9. The adsorption was ascribed to the relatively high surface area (141 $m^2 \cdot g^{-1}$ for the sample pyrolyzed at 600 ºC), hydrophobicity, and potential interaction between biochar and triclosan functional groups including hydrogen bonding and π-stacking. More recently, the same research group analyzed the triclosan adsorption on bench-scale column experiments to stablish the influence of flow rate and competition due to the presence of other organic micropollutants and inorganic nutrients on adsorption on biochar [166].

Pesticides removal from waste by adsorption on biochar has been also analyzed in the literature. Mandal et al. [167] studied the adsorption of atrazine and imidacloprid on different chars obtained from eucalyptus bark, corn cob, bamboo chips, rice husk and rice straw. The adsorption kinetics was well described by the Elovich model. The adsorption capacity of the rice straw derived biochar was enhanced after treatment with phosphoric acid. Atrazine adsorption on biochars obtained from dairy manure by heat treatment in air at different temperatures (⩽500 °C) was also studied) [168]. This study concludes that the removal efficiency increases with the temperature of the treatment, although at the highest temperature the sample showed an extremely high ash content, due to the oxidation of most of the organic matter of the biochar. Zhao et al. [169] analyzed the effect of $NH_4H_2PO_4$ treatment of corn stalk biochars on the atrazine adsorption. They conclude that the treatment increases very

significantly the adsorption capacity of atrazine on biochar, from 7.8 up to 53.9 mg·g^{-1} at 25 ºC. The isotherms were best fitted by the Redlich–Peterson model. Atrazine sorption on deashed pig manure biochars suggested that the adsorption mechanism can be explained by hydrophobicity of the adsorbent, although pore-filling and π–π electron donor–acceptor interactions were also involved [170]. Adsorption increased very significantly with the removal of the ashes, probably by the unblocking of adsorption active sites. Xiao and Pignatello [171] indicated that micro- and mesoporosity of biochars, which increase with the temperature of the synthesis treatment, strongly affect the adsorption of triazine herbicides. Although, steric effects and π–π electron donor-acceptor interactions have also to be considered. Liu et al. [172] found that the atrazine adsorption capacities increased with increasing pore volume of biochars. A thermodynamic analysis revealed a low activation energy of the adsorption process suggesting a predominantly physical adsorption mechanism. The adsorption of several pesticides, namely, bentazone, chlorpyrifos, diuron, glyphosate and 2-methyl-4-chlorophenoxyacetic acid (MCPA) on wood derived biochars was analyzed by Cederlund et al. [173] The adsorption capacity varied greatly depending on the pesticide following the order diuron > chlorpyrifos > MCPA > bentazone > glyphosate. Heat treatment at 450 ºC increased the porosity and the wettability of the biochar, resulting in increased adsorption of MCPA and bentazone. The coating of the biochar with magnetite reduced the specific surface area although enhanced the adsorption of glyphosate.

The adsorption of plasticizers compounds has also been analyzed in the literature. Different biochars from the pyrolysis of grass and wood biomass at different temperatures (200-700 ºC) were used in the adsorption of phthalic acid esters (PAEs) with different hydrophobicity [174]. The study concluded that lower temperature treatments yield more efficient adsorbents as a consequence of their higher hydrophobicity. Jin et al. [175] analyzed the adsorption and co-adsorption of phenanthrene (PHE) and dibutyl phthalate (DBP) on biochars from grass (soybean, rice, and cotton) straw, wood dust and swine manure. They observed enhanced adsorption with surface polarity and ash content, probably due to the increase of polar groups of the inorganic material. The presence of PHE resulted in DBP enhanced adsorption, suggesting that DBP and PHE had different adsorption sites. Ghaffar et al. [176] analyzed the effect of biochar aging on adsorption capacity of di-alkyl phthalates. Biochars were synthesized from peanut-shell and their aging was induced by chemical oxidation with HNO_3/H_2SO_4. Despite the aging process reduced surface area and porosity, an increased adsorption is observed after aging probably due to the existence of strong binding sites between the oxidized surface of the adsorbent and the phthalates molecules. The adsorption proceeds through hydrophobic interactions and π-π electron donor-acceptor interactions. Recently, Jing et al. [177] studied the adsorption of two typical PAEs, dimethyl phthalate and diethyl phthalate, on biochars obtained from peanut hull and wheat straw at different pyrolysis temperatures (450, 550, and 650 °C). Increasing pyrolysis temperatures results in biochar with higher surface area, higher aromaticity and lower amount of surface functional groups. Adsorption kinetics were well defined by quasi-second-order kinetic model. Regarding to the adsorption capacity, the biochars from wheat straw showed higher adsorption capacities than those of peanut hull biochars, probably due to the differences in the oxygen-functional groups.

6.1. Adsorption on activated carbons

Since the removal of emerging contaminants is receiving special attention in the purification of waters, there are many works in bibliography devoted to this line of research. Table 4 summarizes the adsorbed emerging contaminant, some of the characteristic parameters of the activated carbon used as adsorbent, the temperature and pH at which the adsorption process was analyzed and the maximum adsorption capacity (mainly from the Langmuir's monolayer adsorption capacity, but also directly from experimental results) obtained from some of the studies previously reported in the literature.

The adsorption of antibiotics has been widely analyzed. In this sense, Rajapaksha et al. [178] studied the adsorption of sulfamethazine (SMT) from water on steam activated biochars from *Sicyos angulatus L.*, from gourd family. Adsorption showed a strong dependence with pH, surface area and

Peer-reviewed version available at C 2018, 4, 63; doi:10.3390/c4040063

Table 4. Adsorbed emerging contaminant, some of the characteristic parameters of the activated carbon used as adsorbent, temperature and pH at which the adsorption process was analyzed, and maximum adsorption capacity obtained from some of the studies previously reported in the literature.

Pollutant	Activating agent	Biomass precursor	A_{BET} ($m^2 \cdot g^{-1}$)	T (ºC)	pH	Adsorption capacity ($mg \cdot g^{-1}$)***	Ref.
Antibiotics							
Tetracycline	NaOH	Macadamia nut shells	1524	--	3.0–10.0	455.3	[97]
Tetracycline	H_3PO_4	Lignin	933	20	5.5	475.5	[179]
Tetracycline	H_3PO_4	Hazelnut shell	1425	20	5.0	302.9	[180]
Tetracycline	H_3PO_4	Apricot stones	308	30	--	308.3	[181]
Tetracycline	H_3PO_4 – $Fe(NO_3)_3$	*Iris tectorum*	1371	22	2.0-11.0	769.2	[182]
Tetracycline	$ZnCl_2$	Tomato industrial waste	1093	35	5.7	500.0	[183]
Tetracycline	$ZnCl_2$	Grape industrial processing pulps	1455	35	5.7	625.0	[184]
Tetracycline	$ZnCl_2$	Oak charcoals	224	20	3.0-11.0	282.1	[185]
Tetracycline	NaOH	*Pinus taeda*	960	20	6.0	274.8	[98]
Oxytetracycline	H_3PO_4	Hazelnut shell	1425	20	5.0	321.5	[180]
Chlortetracycline	H_3PO_4	Hazelnut shell	1425	20	5.0	313.5	[180]
Sulfamethazine	Steam	*Sicyos angulatus L*		25	3.0	37.7	[178]
Sulfamethoxazole	H_3PO_4	Bleached pulp	965	25	7.3	13.0	[186]
Amoxicillin	$ZnCl_2$	Macauba palm waste	907	25	--	38.0	[187]
Ciprofloxacin	H_3PO_4	Lignin	933	20	5.5	418.6	[179]
Steroids							
Ethinylestradiol	$ZnCl_2$	Macauba palm waste	907	25	3.0-9.0	30.8	[187]
17β-Estradiol	NaOH	Mixture of several biomass waste	16	25	2.0-11-0	7.6	[188]
17α-Ethinylestradiol	NaOH	Mixture of several biomass waste	16	25	2.0-11-0	7.9	[188]
β-blockers							
Atenolol	CO_2	Palm kernel shell	711	25	7.0	183.4	[189]
Acebutolol	CO_2	Palm kernel shell	711	25	7.0	225.4	[189]
Anti-inflammatory							
Ibuprofen	H_3PO_4	Olive-waste cakes	793	20-40	2.0-8.6	12.6	[190]
Ibuprofen	Steam	*Aegle marmelos* shell	308	15-45	2.0-6.0	12.6	[191]
Ibuprofen	K_2CO_3 - steam	Cork waste	1060	20-40	2.0-11-0	416.7	[192]
Naproxen	H_3PO_4	Olive-waste cakes	793	20-40	2.0-8.6	39.5	[190]

Pollutant	Activating agent	Biomass precursor	A_{BET} ($m^2 \cdot g^{-1}$)	T (ºC)	pH	Adsorption capacity ($mg \cdot g^{-1}$)***	Ref.
Ketoprofen	H_3PO_4	Olive-waste cakes	793	20-40	2.0-8.6	24.7	[190]
Diclofenac	H_3PO_4	Olive-waste cakes	793	20-40	2.0-8.6	56.2	[190]
Analgesic							
Paracetamol	H_3PO_4	Olive stones	990	25	--	98.4	[193]
Paracetamol	H_3PO_4	Spent tea leaves	1208	25	7.0	59.2	[194]
Antipyrine	$FeCl_3$	Tara gum	1680	20	--	275.0	[54]
Antiepileptic							
Carbamazepine	H_3PO_4	Bleached pulp	965	25	7.3	92.0	[186]
Carbamazepine	CO_2	Palm kernel shell	711	25	7.0	170.1	[189]
Carbamazepine	KOH	Pomelo peels	904	25	2.0-12.0	286.5	[195]
Carbamazepine	H_3PO_4	Peach stones	1216	30	Natural	335.0	[196]
Stimulant							
Caffeine	$ZnCl_2$ (MW)*	*Eragrostis plana Nees* leaves	1250	25	7.0	235.5	[197]
Caffeine	H_3PO_4	Pineapple leaves	1031	25-55	2.0-9.0	155.5	[198]
Caffeine	KOH	Polymer waste	1889	25	--	351.0	[199]
Pesticide							
Atrazine	KOH	Hemp stem	2213	25	5.0-9.0	466.0	[200]
Atrazine	KOH	Sugarcane bagasse	1325	20-40	3.0-11.0	196.1	[201]
Atrazine	H_3PO_4	Banana peels	--	25-60	2.0-9.0	14.4	[202]
Glyphosate	KOH	Waste newspaper	535	28	2.5-8.0	48.4	[203]
Carbofuran	KOH + CO_2	Palm oil fronds	1237	30	2.0-12.0	164.0	[204]
Diuron	H_3PO_4	Grape seeds	1139	15-45	--	129.1	[205]
Plasticizers							
Dibutyl phthalate	H_3PO_4	*Albizzia julibrissin* pods	1139 $mg \cdot g^{-1}$ IN**	10-40	3.8	1305.0	[206]
Diethyl phthalate	H_3PO_4	*Albizzia julibrissin* pods	1139 $mg \cdot g^{-1}$ IN**	10-40	3.8	457.0	[206]
Dibutyl phthalate	$ZnCl_2$	Ginkgo leaves	697	25	1.0-13.0	129.9	[207]
Dibutyl phthalate	--	Nutshell	1224	25-55	3.0-9.0	104.7	[208]

*MW = Microwave heating; **IN = Iodine number;

***The adsorption capacity corresponds in many of the studies to the monolayer adsorption capacity of the Langmuir isotherm

pore volume. The equilibrium data were well predicted by the Freundlich and Temkin models indicating favorable chemisorption processes and electrostatic interactions between SMT and the surface of the adsorbent. The activation process resulted in an increased adsorption capacity with a maximum at an activation temperature of 700 ºC and pH 3 (37.7 $mg \cdot g^{-1}$). Oliveira et al. [186] prepared activated carbons by chemical activation with K_2CO_3 or H_3PO_4 using raw and bleached pulps from the papermaking industry. The carbons were used as adsorbents in batch-type adsorbers on the removal of the antiepileptic carbamazepine and the antibiotic sulfamethoxazole from ultra-pure water and from Waste Water Treatment Plant (WWTP) effluents. In the case of real WWTP effluents, although the synthesized activated carbons adsorbed significant amounts of both carbamazepine and sulfamethoxazole contaminants, a lower adsorption capacity was obtained for the latter. The highest adsorption capacities from WWTP effluents were achieved by carbons produced from bleached pulp and activated with H_3PO_4, 92.0 and 13.0 $mg \cdot g^{-1}$ for carbamazepine and sulfamethoxazole, respectively. Tetracycline was adsorbed on a NaOH-activated carbon synthesized from macadamia nut shell using an impregnation ratio of 3:1 and an activation temperature of 700 ºC [97]. The porous structure is composed mainly of micropores (78.2%) with a surface area of 1524 $m^2 \cdot g^{-1}$. According to Boehm titration, the surface of the activated carbons presents predominantly basic groups, being in agreement with the pH_{pzc} value of 8.74. The isotherm model that best fitted to experimental data was Temkin, while the best fitted kinetic model was Elovich. The maximum monolayer adsorption capacity was 455.33 mg g^{-1}. The adsorption process is limited by intraparticle and film diffusion. Marzbali et al. [181] studied the batch adsorption of tetracycline using a mesoporous activated carbon prepared from apricot shell by H_3PO_4 activation. A thermodynamic analysis revealed that the adsorption process is endothermic and spontaneous. Adsorption equilibrium data fitted well to the Freundlich model, whereas adsorption kinetics followed a pseudo-second order model. The highest adsorption capacity on this activated carbon was 308.3 $mg \cdot g^{-1}$. The authors concluded that tetracycline adsorption is controlled by both intraparticle diffusion and film diffusion mechanisms. The results showed the successful application of synthesized activated carbon for effective removal of tetracycline (TC). Huang et al. [179] analyzed the adsorption of tetracycline and ciprofloxacin on an activated carbon obtained from lignin by H_3PO_4 chemical activation. The synthesized activated carbon showed a surface area of 933 $m^2 \cdot g^{-1}$ and both acidic and basic surface functional groups. The adsorption kinetics for both adsorbates followed pseudo-second order model, while adsorption equilibrium data adjusted well to the Langmuir isotherm with maximum adsorption capacities of 475.48 and 418.60 $mg \cdot g^{-1}$ for tetracycline and ciprofloxacin, respectively. The effect of ferric nitrate as dopant for adsorption of tetracycline from aqueous solutions was analyzed by Li et al. [182]. Ferric nitrate was used for altering the properties of an activated carbon obtained by H_3PO_4 chemical activation of *Iris tectorum*. The presence of the nitrate salt increases the porous development and the amount of surface acidic groups, resulting in a significantly higher adsorption capacity of tetracycline. A strong reduction of the adsorption capacity with increased pH was observed, with a tetracycline maximum adsorption capacity of 769.2 $mg \cdot g^{-1}$. Fan et al. [180] analyzed the equilibrium and kinetic and sorption of three tetracycline antibiotics, namely, tetracycline (TC), oxytetracycline (OTC), and chlortetracycline (CTC), on hazelnut shell derived activated carbons (HSAC) obtained by H_3PO_4 activation. The maximum adsorption capacities were 321.5, 313.5 and 302.9 $mg \cdot g^{-1}$ for OTC, CTC and TC, respectively. The data fitted well with the pseudo-second-order kinetic and Langmuir models. The intraparticle diffusion model indicated that the adsorption of TCs on the HSAC was controlled by both intraparticle diffusion and external mass transfer. Under the tested temperature and pressure, the thermodynamic constants revealed that the adsorption of TCs onto the HSAC was spontaneous and endothermic. Sayğılı and Güzel [183] synthesized an activated carbon by $ZnCl_2$-activation of tomato industrial processing waste devoted to tetracycline adsorption. The experimental data followed a pseudo-second order kinetic model and the Langmuir isotherm, with a maximum adsorption capacity of 500.0 $mg \cdot g^{-1}$. Thermodynamic study reveals that the adsorption was endothermic and spontaneous under the analyzed conditions. In a similar study [184], the same authors obtained even a higher adsorption capacity of tetracycline, 625 $mg \cdot g^{-1}$, using an activated carbon prepared by $ZnCl_2$ chemical activation from grape industrial processing pulps. $ZnCl_2$ was also

chosen as activating agent for the preparation of an activated carbon from oak charcoals devoted to tetracycline adsorption [185]. In this study, the effect of the presence of inorganic cations (Li^+, K^+, Mg^{2+}, Ca^{2+}, Ni^{2+}, and Fe^{3+}) and anions (HCO_3^-, NO_3^- and SO_4^{2-}) was analyzed, resulting in all cases in a reduction of the tetracycline amount adsorbed. Conversely, in this study, the solution pH showed very little effect on the adsorption. The highest amount adsorbed was 282.1 $mg \cdot g^{-1}$. Jang el al. [98] evaluated the adsorption of tetracycline on NaOH activated carbon from *Pinus taeda*. The study concluded that hydrogen bonding and π-π interaction were the most plausible adsorption mechanisms, being intraparticle diffusion a major limitation for the adsorption.

The adsorption of five endocrine disruptors, namely estrone (E1), 17β-estradiol (E2), estriol (E3), 17α-ethynylestradiol (EE2) and bisphenol A (BPA) on carbon from Eucalyptus globulus wood particles activated with H_3PO_4 was analyzed by Ahmed et al. [209]. The authors concluded that π-π-electron-donor-acceptor interactions were responsible of the adsorption mechanism. The adsorption capacity decreased following the order E1 > E2 > EE2 > E3 > BPA. Moura et al. [187] analyzed the adsorption of bisphenol A, ethinylestradiol, and amoxicillin on an activated carbon obtained by chemical activation with $ZnCl_2$ of Macauba palm waste. The N_2 adsorption-desorption isotherms at -196 ºC revealed a porosity consisting of micropores and narrow mesopores with a total surface area of 907 $m^2 \cdot g^{-1}$. The highest adsorption capacities were 33.8, 30.8 and 26.3 $mg \cdot g^{-1}$ for bisphenol A, ethinylestradiol and amoxicillin, respectively. The authors also analyzed the effect of the pH and the possible adsorption mechanisms. In the case of bisphenol-A, the fact that the adsorption is not altered by positive or negative surface charges, and the molecule has two aromatic rings with conjugated π bonds, suggested that the mechanism of π-π interactions was the most probable. Similar results were observed in ethinylestradiol adsorption. In contrast, amoxicillin showed an increase in the adsorbed amount at pH of 3, where a positive surface charge is present, suggesting an electrostatic interaction mechanism. Rovani et al. [188] obtained an activated carbon from NaOH activation of coffee grounds, eucalyptus sawdust and soybean oil. The carbon, with a very limited porosity development (16 $m^2 \cdot g^{-1}$) was used as adsorbent of 17β-estradiol (E2) and 17α-ethinylestradiol (EE2) from aqueous solutions. The kinetic experimental points were well described by a general order kinetic model, whereas equilibrium points were best fitted by Sips isotherm model. The maximum adsorption capacities were 7.6 and 7.9 $mg \cdot g^{-1}$ for E2 and EE2, respectively. The adsorption behavior of both compounds was very similar regardless of the adsorption conditions.

Mestre el al [192] synthesized activated carbons from cork waste by two different procedures, chemical activation with K_2CO_3, and by a two stages procedure constituted by a chemical activation with K_2CO_3 followed by a steam activation. The carbons were used for the adsorption of ibuprofen from water. The steam activation step yields an activated carbon with a larger volume of supermicropores and less acidic groups, resulting in significantly higher adsorption capacity of ibuprofen. Again, as in many studies considered, kinetic and equilibrium adsorption results were in agreement with the pseudo-second order kinetic equation and Langmuir model. Between 25 and 40 ºC no significant influence of the temperature on ibuprofen adsorption was observed, reaching a maximum adsorbed amount of 416.7 $mg \cdot g^{-1}$. However, the amount adsorbed decreases strongly with increasing pH of the solution. The same research group [210] used activated carbon adsorbents obtained from chemical and physical activation of a bioresource (cork) and a municipal waste (plastic) also for ibuprofen removal. The work indicated that the ibuprofen adsorption is favored when using activated carbons with basic surface properties and formed by mesopores and micropores, whose presence is crucial to ensure accessibility and accommodation of the ibuprofen molecule. Mondal et al. [211] explored the ibuprofen adsorption of steam activated mung bean husk biochar. The equilibrium adsorption data followed the Langmuir isotherm model (maximum adsorption capacity 62.5 $mg \cdot g^{-1}$), whereas kinetic results fitted well a pseudo second order model. Chakraborty et al. [191] studied the ibuprofen uptake on raw and steam activated biochar of *Aegle marmelos* shell. Ibuprofen sorption by raw and steam-activated carbons followed Langmuir and Freundlich isotherms respectively, following a pseudo second order kinetic model for both pollutants. The thermodynamic study suggested the process to be exothermic, spontaneous and feasible in nature. Baccar et al. [190] analyzed the adsorption of different pharmaceuticals, namely,

ibuprofen, ketoprofen, naproxen and diclofenac on activated carbon synthesized by H_3PO_4 chemical activation of olive-waste cakes. Single and mixture drug solutions were considered. The adsorption capacities of the four contaminants were quite different and relate to their pKa and their octanol/water coefficients. The adsorption kinetics followed the pseudo-second-order kinetic model for the four drugs. Increasing pH gradually reduced the adsorption capacities of the four compounds. In contrast, adsorption temperature shows negligible effect in the adsorption process.

Wong et al. [194] synthesized activated carbons from spent tea leaves by chemical activation with $ZnCl_2$, H_3PO_4, NaOH and K_2CO_3 for the adsorption of paracetamol. The activated carbon prepared with H_3PO_4 showed the highest paracetamol adsorption capacities (59.2 $mg \cdot g^{-1}$) probably as a consequence of the more proper activation conditions for this activating agent (impregnation ratio 1:1 and activation temperature 600 ºC). The adsorption equilibrium results followed the Langmuir isotherm model, whereas adsorption kinetics obeyed the pseudo-second order model. Garcia-Mateos et al. [193] reported one of the very few studies about adsorption of emerging contaminants on biomass-derived carbons in fixed-bed adsorbers. In this study, paracetamol was adsorbed on an activated carbon synthesized by H_3PO_4 activation of olive stone waste. Equilibrium results fitted well to Langmuir isotherms with maximum adsorption capacities of around 100 $mg \cdot g^{-1}$ depending on the adsorption temperature. Breakthrough adsorption curves were predicted from the batch kinetics experiments after estimation of homogeneous and heterogeneous diffusion coefficients, reflecting the dependence of diffusion with the surface coverage of paracetamol. Bedia et al. [54] synthesized activated carbons from Tara gum by the less studied $FeCl_3$ activation. Activation temperatures in the range of 400 to 1000 °C and different impregnation ratios were used. The highest surface area reaches 1680 $m^2 \cdot g^{-1}$ with predominance of micropores (≈75%). The carbons were tested for the aqueous-phase adsorption of antipyrine. The kinetic curves and adsorption isotherms fitted well to hyperbolic and Langmuir equations, respectively. At 20 °C, the saturation adsorption capacity was 275 $mg \cdot g^{-1}$. In this study, the adsorption capacity of the different synthesized activated carbons seems to be basically determined by the surface area of the carbons, although some deviations are observed probably provoked by the different amount of surface functionalities, essentially oxygen bearing groups.

In a recent study, Chen et al. [195] reported the adsorption of carbamazepine from water on activated carbons synthesized by means of chemical activation with KOH of pomelo peels. Kinetic results fitted to pseudo-second-order kinetics and controlled by the intra-particle diffusion. Equilibrium experimental point were well described by the Langmuir model isotherm. The maximum carbamazepine adsorption capacity was 286.5 $mg \cdot g^{-1}$. The study concludes that both the porous development and the amount of surface functional groups affect the adsorption. The adsorption process was spontaneous and exothermic, and mainly of physisorption type. It was stated that the adsorption mechanism of carbamazepine on the synthesized activated carbons was mainly controlled by π–π electron donor–acceptor interactions. To et al. [189] studied the adsorption the antiepileptic carbamazepine and two β-blockers, atenolol and acebutolol, on an activated carbon synthesize from palm kernel shell by physically activation with carbon dioxide at 900 °C. The kinetic tests suggested the adsorption proceeds predominantly by chemisorption mechanism (in contrast with the observed by Chen et al. [195]) following the Ritchie-second-order kinetic model. The equilibrium results were adjusted by the Sips equation with maximum adsorption capacities of 183.4, 225.4 and 170.1 $mg \cdot g^{-1}$ for atenolol, acebutolol and carbamazepine, respectively. Torrellas et al. [196] studied the batch and dynamic adsorption of caffeine, diclofenac and carbamazepine on activated carbons obtained from peach stones by chemical activation with H_3PO_4. The carbons were submitted to different thermal treatments in presence and absence of oxygen to understand the effect of surface groups on the adsorption process. It was observed that the oxidation of the carbon surface decreased very significantly the adsorption capacity as a consequence of the enhancement of the hydrophobicity. The maximum carbamazepine adsorption capacity (355 $mg \cdot g^{-1}$) was higher than those of caffeine and diclofenac, probably as a consequence of its more hydrophobic character and higher water solubility.

Eragrostis plana Nees leaves were used as precursor for synthesizing an activated carbon by using microwave-assisted pyrolysis and chemical activation with $ZnCl_2$ [197]. The synthesized activated carbon was devoted to the adsorption of caffeine and 2-nitrophenol from water. The activation yielded a predominantly mesoporous carbon with a high surface area value of 1250 $m^2 \cdot g^{-1}$. FTIR analysis suggested the existence of carboxylic, carbonyl and hydroxyl functional groups on the carbon surface, whereas Boehm tritation revealed a high amount of acid moieties. The highest adsorption capacities of caffeine and 2-nitrophenol adsorbed at 25 °C were 235.5 and 255.8 mg g^{-1}, respectively. Recently, Beltrame et al. [198] analyzed the preparation of activated carbon fibers by H_3PO_4-activation of pineapple plant leaves for the adsorption of caffeine from water. The activated fiber showed a surface area of 1031 $m^2 \cdot g^{-1}$ with a high amount of acidic-surface groups from the H_3PO_4 activation process [212,213]. According to thermodynamics, the adsorption is of physisorption nature, exothermic and spontaneous. Sarıcı-Özdemir and Önal [199] analyzed the adsorption of caffeine in active carbons prepared from polymer waste from the textile industry by KOH chemical activation at different impregnation ratios. The highest pours development was obtained at the highest impregnation ratio analyzed, 5:1, resulting an activated carbon with a very high surface area (1889 $m^2 \cdot g^{-1}$) although an extremely low activation yield (3.9%). The work reported a maximum caffeine adsorption capacity on this carbon of 351.0 $mg \cdot g^{-1}$.

The adsorption of pesticides has also received attention in the literature. Lupul et al. [200] reported the adsorption of atrazine on hemp stem-based activated carbons with different surface modification. The activated carbons were synthesized by chemical activation with KOH and their surface chemistry was subsequently modified by thermal annealing, nitric acid oxidation and amination. By these procedures, the authors achieve different carbon adsorbents with very similar porous structure but different surface chemistry. It was concluded that the oxygen and nitrogen functionalities decreased the amount of antipyrine adsorbed. The hydrophobicity of the carbon surface enhanced the adsorption that seems to proceed through π–π dispersive interactions between the atrazine ring and the graphene layers of carbon. Equilibrium results were well fitted by Langmuir and Freundlich-Langmuir isotherms, whereas kinetic data followed intraparticle diffusion mechanism with a noticeable influence of film diffusion. Chang et al. [201] also analyzed the adsorption of atrazine on activated carbons obtained by KOH-activation of sugarcane bagasse. The authors analyzed the effect of pH and temperature on the atrazine adsorption capacities and concluded that pH modification shows very little effect in the adsorption capacity, while the increase of the adsorption temperature results in a slight lower adsorption capacity of atrazine. Chaparadza and Hossenlopp [202] analyzed the kinetics and thermodynamics of atrazine adsorption on an activated carbon synthesized by H_3PO_4 activation using banana peels. In contrast with the reported by Chang et al. [201], in this study there was an optimum pH for atrazine adsorption between 7.0 and 8.2 and the amount of atrazine adsorbed increased with the adsorption temperature in the range analyzed (25-60 ºC). Equilibrium results followed Langmuir and Redlich-Peterson models, while kinetics seemed to be controlled by both external mass transfer and intraparticle diffusion mechanisms. The enthalpy of atrazine adsorption was estimated to be 67.8 $kJ \cdot mol^{-1}$ with a Gibbs free energy of -5.7 $kJ \cdot mol^{-1}$. Nourouzi et al. [203] analyzed the adsorption of glyphosate on activated carbon from waste newspaper. The activated carbon was obtained by a modified KOH-activation process, resulting in a relatively low porosity carbon with a total surface area equal to 535 $m^2 \cdot g^{-1}$. The amount adsorbed decreased very significantly with the pH, with a maximum adsorption capacity of glyphosate of 48.4 $mg \cdot g^{-1}$. The adsorption of the herbicide bentazon [101] and the insecticide carbofuran [204] on activated carbon obtained from palm oil fronds by means of a physico-chemical activation method, which consisted of a simultaneous activation with KOH and CO_2 gasification. The maximum surface area obtained was 1237 $m^2 \cdot g^{-1}$. The adsorption of carbofuran fitted well to Langmuir model isotherm. The regeneration of the spent activated carbon was also analyzed with good results. Al Bahri et al. [205] synthesized activated carbons from grape seeds by chemical activation with phosphoric acid devoted to the adsorption of diuron from water. This study analyzed the effect of the activation temperature and impregnation ratio on the porous development of the resulting activated carbons. The best results in terms of surface area and mesopore volume

development were obtained using an impregnation ratio of 3:1 and a carbonization temperature of 500 °C. Among the different kinetic model analyzed, the pseudo-second-order described better the experimental results.

The removal of plasticizers is also under study using activated carbons from various sources. So for example, Bouhamidi et al. [206] analyzed the adsorption of diethyl and dibutyl phthalates on an activated carbon obtained from *Albizzia julibrissin* pods by H_3PO_4 chemical activation. Equilibrium results were best fitted by Langmuir models with maximum adsorption capacities at 20 ºC equal to 977 and 438 $mg \cdot g^{-1}$ for dibutyl and diethyl phthalate, respectively. Kinetic data followed well a pseudo-second-order model, whereas adsorption seemed to proceed by a liquid film diffusion mechanism. The adsorption of the two phthalates followed the same trend attended although with higher adsorption capacities for the butyl than for the ethyl phthalate. Wang and Chen [207] reported the adsorption of dibutyl phthalate from aqueous solution using ginkgo leaves-activated carbon by chemical activation with zinc chloride. Equilibrium data were well described by Freundlich isotherm model, whereas kinetic data fitted well to the pseudo-second-order model. The experimental maximum adsorption capacity of dibutyl phthalate was 48.7 $mg \cdot g^{-1}$ at pH 13, while the monolayer adsorption capacity quantified by the Langmuir isotherm was 129.9 $mg \cdot g^{-1}$. According to a thermodynamic analysis, the adsorption was thermodynamically feasible and spontaneous. Fang and Huang [208] studied the adsorption of di-N-butyl phthalate on a commercial nutshell-derived activated carbon with a maximum adsorption capacity of 104.7 $mg \cdot g^{-1}$ at 45 ºC and pH between 5 and 7. Adsorption isotherms correlate well with the Freundlich model, specially at lower initial concentrations of di-N-butyl phthalate. Kinetic data at different adsorption conditions followed a pseudo-first-order model. The adsorption rate was controlled by both film and pore diffusion. The authors observed an increase of the adsorption capacity with the adsorption temperature. A thermodynamic study revealed that the adsorption process was endothermic and spontaneous.

Jung et al [214] analyzed the adsorption of several endocrine disrupting compounds (bisphenolA, atrazine and 17 β-ethinylestradiol) and pharmaceuticals (sulfamethoxazole, carbamazepine, diclofenac and ibuprofen) on activated biochars (more properly, activated carbons). The adsorbents were synthesized by chemical activation with NaOH of loblolly pine chips under oxygenated and oxygen-free conditions. The carbon synthesized under oxidizing conditions was composed mostly of aromatic moieties, with lower H/C and O/C ratios than the prepared in the absence of oxygen, which showed many polar functional groups. The higher development of porosity of the carbon obtained in free-oxygen environment resulted in higher adsorption capacity for all the compounds analyzed.

7. Conclusion and outlooks

The presence of emerging contaminants in water will be very likely a problem of growing importance in the years to come. Therefore, the search for new technologies or the development of the existing ones is of crucial to assure a safe and continuous water supply. In addition, due to the resources and energy shortage, these processes and technologies analyzed must be economically and environmentally sustainable. In this context, the current review highlights the enormous potential of biomass waste to be used as precursors for the synthesis of biochars or activated carbons for the adsorption of emerging contaminants. The benefits of this approach include the use and valorization of the biomass resources or the efficient purification of contaminated water, all framed within an environmentally friendly process at a relatively low cost. This review summarizes the abundant opportunities dealing with the reuse of waste for the manufacture of adsorbents and their application in water purification. To go further in this field, researchers have to find ways of implementing these adsorbents at industrial scale. Therefore, the fundamental understanding of the adsorbent properties and the adsorption mechanism will help in the exploration of process scale-up.

Acknowledgments: The authors acknowledge the financial support from Spanish MINECO (project CTQ2016-78576-R). M. Peñas-Garzón is indebted to Spanish MECD for FPU16/00576 predoctoral contract.

Conflicts of Interest: The authors declare no conflict of interest.

References

1. Taheran, M.; Naghdi, M.; Brar, S. K.; Verma, M.; Surampalli, R. Y. Emerging contaminants: Here today, there tomorrow! *Environ. Nanotechnology, Monit. Manag.* **2018**, *10*, 122–126, doi:10.1016/J.ENMM.2018.05.010.
2. Zhao, L.; Deng, J.; Sun, P.; Liu, J.; Ji, Y.; Nakada, N.; Qiao, Z.; Tanaka, H.; Yang, Y. Nanomaterials for treating emerging contaminants in water by adsorption and photocatalysis: Systematic review and bibliometric analysis. *Sci. Total Environ.* **2018**, *627*, 1253–1263, doi:10.1016/j.scitotenv.2018.02.006.
3. Farré, M. la; Pérez, S.; Kantiani, L. Fate and toxicity of emerging pollutants, their metabolites and transformation products in the aquatic environment. *TrAC Trends Anal. Chem.* **2008**, *27*, 991–1007, doi:10.1016/J.TRAC.2008.09.010.
4. Luo, Y.; Guo, W.; Ngo, H. H.; Nghiem, L. D.; Hai, F. I.; Zhang, J.; Liang, S.; Wang, X. C. A review on the occurrence of micropollutants in the aquatic environment and their fate and removal during wastewater treatment. *Sci. Total Environ.* **2014**, *473–474*, 619–641, doi:10.1016/J.SCITOTENV.2013.12.065.
5. Rodriguez-Narvaez, O. M.; Peralta-Hernandez, J. M.; Goonetilleke, A.; Bandala, E. R. Treatment technologies for emerging contaminants in water: A review. *Chem. Eng. J.* **2017**, *323*, 361–380, doi:10.1016/J.CEJ.2017.04.106.
6. Sipma, J.; Osuna, B.; Collado, N.; Monclús, H.; Ferrero, G.; Comas, J.; Rodriguez-Roda, I. Comparison of removal of pharmaceuticals in MBR and activated sludge systems. *Desalination* **2010**, *250*, 653–659, doi:10.1016/J.DESAL.2009.06.073.
7. Carr, D. L.; Morse, A. N.; Zak, J. C.; Anderson, T. A. Biological Degradation of Common Pharmaceuticals and Personal Care Products in Soils with High Water Content. *Water, Air, Soil Pollut.* **2011**, *217*, 127–134, doi:10.1007/s11270-010-0573-z.
8. Matamoros, V.; Sala, L.; Salvadó, V. Evaluation of a biologically-based filtration water reclamation plant for removing emerging contaminants: A pilot plant study. *Bioresour. Technol.* **2012**, *104*, 243–249, doi:10.1016/J.BIORTECH.2011.11.036.
9. Sui, Q.; Huang, J.; Deng, S.; Chen, W.; Yu, G. Seasonal Variation in the Occurrence and Removal of Pharmaceuticals and Personal Care Products in Different Biological Wastewater Treatment Processes. *Environ. Sci. Technol.* **2011**, *45*, 3341–3348, doi:10.1021/es200248d.
10. Wang, Y.-K.; Sheng, G.-P.; Shi, B.-J.; Li, W.-W.; Yu, H.-Q. A Novel Electrochemical Membrane Bioreactor as a Potential Net Energy Producer for Sustainable Wastewater Treatment. *Sci. Rep.* **2013**, *3*, 1864, doi:10.1038/srep01864.
11. Ma, J.; Wang, Z.; Mao, B.; Zhan, J.; Wu, Z. Electrochemical Membrane Bioreactors for Sustainable Wastewater Treatment: Principles and Challenges. *Curr. Environ. Eng.* **2015**, *2*, 38–49, doi:10.2174/2212717802011503 31145842.
12. Andreozzi, R.; Caprio, V.; Insola, A.; Marotta, R. Advanced oxidation processes (AOP) for water purification and recovery. *Catal. Today* **1999**, *53*, 51–59, doi:10.1016/S0920-5861(99)00102-9.
13. Freyria, F.; Geobaldo, F.; Bonelli, B.; Freyria, F. S.; Geobaldo, F.; Bonelli, B. Nanomaterials for the Abatement of Pharmaceuticals and Personal Care Products from Wastewater. *Appl. Sci.* **2018**, *8*, 170, doi:10.3390/app8020170.
14. Krauskopf, L. G. Plasticizer structure/performance relationships. *J. Vinyl Addit. Technol.* **1993**, *15*, 140–147, doi:10.1002/vnl.730150306.
15. Ali, I.; Gupta, V. K. Advances in water treatment by adsorption technology. *Nat. Protoc.* **2007**, *1*, 2661–2667, doi:10.1038/nprot.2006.370.

16. Singh, N. B.; Nagpal, G.; Agrawal, S.; Rachna Water purification by using Adsorbents: A Review. *Environ. Technol. Innov.* **2018**, *11*, 187–240, doi:10.1016/J.ETI.2018.05.006.
17. Uddin, M. K. A review on the adsorption of heavy metals by clay minerals, with special focus on the past decade. *Chem. Eng. J.* **2017**, *308*, 438–462, doi:10.1016/J.CEJ.2016.09.029.
18. Wang, S.; Peng, Y. Natural zeolites as effective adsorbents in water and wastewater treatment. *Chem. Eng. J.* **2010**, *156*, 11–24, doi:10.1016/j.cej.2009.10.029.
19. Khan, N. A.; Hasan, Z.; Jhung, S. H. Adsorptive removal of hazardous materials using metal-organic frameworks (MOFs): A review. *J. Hazard. Mater.* **2013**, *244–245*, 444–456, doi:10.1016/j.jhazmat.2012.11.011.
20. Jeirani, Z.; Niu, C. H.; Soltan, J. Adsorption of emerging pollutants on activated carbon. *Rev. Chem. Eng.* **2017**, *33*, 491–522, doi:10.1515/revce-2016-0027.
21. Gwenzi, W.; Chaukura, N.; Noubactep, C.; Mukome, F. N. D. Biochar-based water treatment systems as a potential low-cost and sustainable technology for clean water provision. *J. Environ. Manage.* **2017**, *197*, 732–749, doi:10.1016/J.JENVMAN.2017.03.087.
22. Rabaçal, M., Ferreira, A.F., Silva, C.A.M., Costa, M. *Biorefineries*; Rabaçal, M., Ferreira, A. F., Silva, C. A. M., Costa, M., Eds.; Lecture Notes in Energy; Springer International Publishing: Cham, 2017; Vol. 57; ISBN 978-3-319-48286-6.
23. Bhaskar, T.; Pandey, A.; Mohan, S. V.; Lee, D. J. (Duu-J.; Khanal, S. K. *Waste biorefinery : potential and perspectives*; Elsevier, 2018; ISBN 9780444639936.
24. Shahbazali, E. Biorefinery: from biomass to chemicals and fuels. *Green Process. Synth.* **2013**, *2*, 87–88, doi:10.1515/gps-2012-0094.
25. Demirbaş, A. Biomass resource facilities and biomass conversion processing for fuels and chemicals. *Energy Convers. Manag.* **2001**, *42*, 1357–1378, doi:10.1016/S0196-8904(00)00137-0.
26. de Wit, M.; Faaij, A. European biomass resource potential and costs. *Biomass and Bioenergy* **2010**, *34*, 188–202, doi:10.1016/j.biombioe.2009.07.011.
27. Blanco-Canqui, H. Growing Dedicated Energy Crops on Marginal Lands and Ecosystem Services. *Soil Sci. Soc. Am. J.* **2016**, *80*, 845, doi:10.2136/sssaj2016.03.0080.
28. Glithero, N. J.; Wilson, P.; Ramsden, S. J. Optimal combinable and dedicated energy crop scenarios for marginal land. *Appl. Energy* **2015**, *147*, 82–91, doi:10.1016/j.apenergy.2015.01.119.
29. Dessbesell, L.; Xu, C. (Charles); Pulkki, R.; Leitch, M.; Mahmood, N. Forest biomass supply chain optimization for a biorefinery aiming to produce high-value bio-based materials and chemicals from lignin and forestry residues: a review of literature. *Can. J. For. Res.* **2017**, *47*, 277–288, doi:10.1139/cjfr-2016-0336.
30. Gregg, J. S.; Smith, S. J. Global and regional potential for bioenergy from agricultural and forestry residue biomass. *Mitig. Adapt. Strateg. Glob. Chang.* **2010**, *15*, 241–262, doi:10.1007/s11027-010-9215-4.
31. Scarlat, N.; Martinov, M.; Dallemand, J.-F. Assessment of the availability of agricultural crop residues in the European Union: Potential and limitations for bioenergy use. *Waste Manag.* **2010**, *30*, 1889–1897, doi:10.1016/j.wasman.2010.04.016.
32. Monforti, F.; Bódis, K.; Scarlat, N.; Dallemand, J.-F. The possible contribution of agricultural crop residues to renewable energy targets in Europe: A spatially explicit study. *Renew. Sustain. Energy Rev.* **2013**, *19*, 666–677, doi:10.1016/j.rser.2012.11.060.
33. Ward, A. J.; Lewis, D. M.; Green, F. B. Anaerobic digestion of algae biomass: A review. *Algal Res.* **2014**, *5*, 204–214, doi:10.1016/j.algal.2014.02.001.

34. Bhatnagar, A.; Chinnasamy, S.; Singh, M.; Das, K. C. Renewable biomass production by mixotrophic algae in the presence of various carbon sources and wastewaters. *Appl. Energy* **2011**, *88*, 3425–3431, doi:10.1016/j.apenergy.2010.12.064.
35. Cheng, H.; Hu, Y. Municipal solid waste (MSW) as a renewable source of energy: Current and future practices in China. *Bioresour. Technol.* **2010**, *101*, 3816–3824, doi:10.1016/j.biortech.2010.01.040.
36. Albert, J.; Jess, A.; Kern, C.; Pöhlmann, F.; Glowienka, K.; Wasserscheid, P. Formic Acid-Based Fischer–Tropsch Synthesis for Green Fuel Production from Wet Waste Biomass and Renewable Excess Energy. *ACS Sustain. Chem. Eng.* **2016**, *4*, 5078–5086, doi:10.1021/acssuschemeng.6b01531.
37. Albert, J.; Wasserscheid, P. Expanding the scope of biogenic substrates for the selective production of formic acid from water-insoluble and wet waste biomass. *Green Chem.* **2015**, *17*, 5164–5171, doi:10.1039/C5GC01474C.
38. Karakaş, C.; Özçimen, D.; İnan, B. Potential use of olive stone biochar as a hydroponic growing medium. *J. Anal. Appl. Pyrolysis* **2017**, *125*, 17–23, doi:10.1016/j.jaap.2017.05.005.
39. Kula, I.; Uğurlu, M.; Karaoğlu, H.; Çelik, A. Adsorption of Cd(II) ions from aqueous solutions using activated carbon prepared from olive stone by $ZnCl_2$ activation. *Bioresour. Technol.* **2008**, *99*, 492–501, doi:10.1016/j.biortech.2007.01.015.
40. Ubago-Pérez, R.; Carrasco-Marín, F.; Fairén-Jiménez, D.; Moreno-Castilla, C. Granular and monolithic activated carbons from KOH-activation of olive stones. *Microporous Mesoporous Mater.* **2006**, *92*, 64–70, doi:10.1016/j.micromeso.2006.01.002.
41. Chen, Y.; Zhu, Y.; Wang, Z.; Li, Y.; Wang, L.; Ding, L.; Gao, X.; Ma, Y.; Guo, Y. Application studies of activated carbon derived from rice husks produced by chemical-thermal process—A review. *Adv. Colloid Interface Sci.* **2011**, *163*, 39–52, doi:10.1016/j.cis.2011.01.006.
42. Lin, L.; Zhai, S.-R.; Xiao, Z.-Y.; Song, Y.; An, Q.-D.; Song, X.-W. Dye adsorption of mesoporous activated carbons produced from NaOH-pretreated rice husks. *Bioresour. Technol.* **2013**, *136*, 437–443, doi:10.1016/j.biortech.2013.03.048.
43. Tsai, W.-T.; Jiang, T.-J. Mesoporous activated carbon produced from coconut shell using a single-step physical activation process. *Biomass Convers. Biorefinery* **2018**, *8*, 711–718, doi:10.1007/s13399-018-0322-x.
44. Wu, W.; Li, J.; Lan, T.; Müller, K.; Niazi, N. K.; Chen, X.; Xu, S.; Zheng, L.; Chu, Y.; Li, J.; Yuan, G.; Wang, H. Unraveling sorption of lead in aqueous solutions by chemically modified biochar derived from coconut fiber: A microscopic and spectroscopic investigation. *Sci. Total Environ.* **2017**, *576*, 766–774, doi:10.1016/j.scitotenv.2016.10.163.
45. Jain, A.; Balasubramanian, R.; Srinivasan, M. P. Production of high surface area mesoporous activated carbons from waste biomass using hydrogen peroxide-mediated hydrothermal treatment for adsorption applications. *Chem. Eng. J.* **2015**, *273*, 622–629, doi:10.1016/j.cej.2015.03.111.
46. Tan, I. A. W.; Ahmad, A. L.; Hameed, B. H. Adsorption of basic dye on high-surface-area activated carbon prepared from coconut husk: Equilibrium, kinetic and thermodynamic studies. *J. Hazard. Mater.* **2008**, *154*, 337–346, doi:10.1016/j.jhazmat.2007.10.031.
47. Yang, E.; Yao, C.; Liu, Y.; Zhang, C.; Jia, L.; Li, D.; Fu, Z.; Sun, D.; Robert Kirk, S.; Yin, D. Bamboo-derived porous biochar for efficient adsorption removal of dibenzothiophene from model fuel. *Fuel* **2018**, *211*, 121–129, doi:10.1016/j.fuel.2017.07.099.
48. Hameed, B. H.; Din, A. T. M.; Ahmad, A. L. Adsorption of methylene blue onto bamboo-based activated carbon: Kinetics and equilibrium studies. *J. Hazard. Mater.* **2007**, *141*, 819–825, doi:10.1016/j.jhazmat.2006.07.049.

49. Bedia, J.; Rodríguez-Mirasol, J.; Cordero, T. Water vapour adsorption on lignin-based activated carbons. *J. Chem. Technol. Biotechnol.* **2007**, *82*, doi:10.1002/jctb.1698.
50. Cordero, T.; Rodríguez-Mirasol, J.; Bedia, J.; Rodríguez, J. J. Preparation of carbon materials from lignin. *Opt. Pura y Apl.* **2007**, *40*.
51. Rodríguez-Mirasol, J.; Bedia, J.; Cordero, T.; Rodríguez, J. Influence of water vapor on the adsorption of VOCs on lignin-based activated carbons. *Sep. Sci. Technol.* **2005**, *40*, doi:10.1080/01496390500385277.
52. Gonzalez-Serrano, E.; Cordero, T.; Rodriguez-Mirasol, J.; Cotoruelo, L.; Rodriguez, J. J. Removal of water pollutants with activated carbons prepared from H_3PO_4 activation of lignin from kraft black liquors. *Water Res.* **2004**, *38*, 3043–3050, doi:10.1016/j.watres.2004.04.048.
53. Yamashita, A.; Yoshida, T.; Hidaka, A.; Oshima, T.; Baba, Y. Preparation of activated carbons with high specific surface areas using lignin and crab shells, and their use in methane adsorption. *Carbon N. Y.* **2015**, *93*, 1080, doi:10.1016/j.carbon.2015.07.021.
54. Bedia, J.; Belver, C.; Ponce, S.; Rodriguez, J. J.; Rodriguez, J. J. Adsorption of antipyrine by activated carbons from FeCl3-activation of Tara gum. *Chem. Eng. J.* **2018**, *333*, 58–65, doi:10.1016/j.cej.2017.09.161.
55. Kazmierczak-Razna, J.; Nowicki, P.; Pietrzak, R. Coniferous Wood Sawdust-based Activated Carbons as Adsorbents Obtained with the Use of Microwave Radiation. *J. Wood Chem. Technol.* **2018**, *38*, 286–299, doi:10.1080/02773813.2018.1455705.
56. Mohan, D.; Pittman, C. U.; Bricka, M.; Smith, F.; Yancey, B.; Mohammad, J.; Steele, P. H.; Alexandre-Franco, M. F.; Gómez-Serrano, V.; Gong, H. Sorption of arsenic, cadmium, and lead by chars produced from fast pyrolysis of wood and bark during bio-oil production. *J. Colloid Interface Sci.* **2007**, *310*, 57–73, doi:10.1016/j.jcis.2007.01.020.
57. Ao, W.; Fu, J.; Mao, X.; Kang, Q.; Ran, C.; Liu, Y.; Zhang, H.; Gao, Z.; Li, J.; Liu, G.; Dai, J. Microwave assisted preparation of activated carbon from biomass: A review. *Renew. Sustain. Energy Rev.* **2018**, *92*, 958–979, doi:10.1016/j.rser.2018.04.051.
58. Yang, K.; Peng, J.; Srinivasakannan, C.; Zhang, L.; Xia, H.; Duan, X. Preparation of high surface area activated carbon from coconut shells using microwave heating. *Bioresour. Technol.* **2010**, *101*, 6163–6169, doi:10.1016/J.BIORTECH.2010.03.001.
59. Yuen, F. K.; Hameed, B. H. Recent developments in the preparation and regeneration of activated carbons by microwaves. *Adv. Colloid Interface Sci.* **2009**, *149*, 19–27, doi:10.1016/j.cis.2008.12.005.
60. Ahmed, M. J. Application of agricultural based activated carbons by microwave and conventional activations for basic dye adsorption: Review. *J. Environ. Chem. Eng.* **2016**, *4*, 89–99, doi:10.1016/j.jece.2015.10.027.
61. Hu, B.; Wang, K.; Wu, L.; Yu, S.-H.; Antonietti, M.; Titirici, M.-M. Engineering Carbon Materials from the Hydrothermal Carbonization Process of Biomass. *Adv. Mater.* **2010**, *22*, 813–828, doi:10.1002/adma.200902812.
62. Sevilla, M.; Fuertes, A. B. The production of carbon materials by hydrothermal carbonization of cellulose. *Carbon N. Y.* **2009**, *47*, 2281–2289, doi:10.1016/J.CARBON.2009.04.026.
63. Lucian, M.; Volpe, M.; Gao, L.; Piro, G.; Goldfarb, J. L.; Fiori, L. Impact of hydrothermal carbonization conditions on the formation of hydrochars and secondary chars from the organic fraction of municipal solid waste. *Fuel* **2018**, *233*, 257–268, doi:10.1016/j.fuel.2018.06.060.
64. Nguyen, T. T. N.; Xu, C.-Y.; Tahmasbian, I.; Che, R.; Xu, Z.; Zhou, X.; Wallace, H. M.; Bai, S. H. Effects of biochar on soil available inorganic nitrogen: A review and meta-analysis. *Geoderma* **2017**, *288*, 79–96, doi:10.1016/J.GEODERMA.2016.11.004.

65. Liu, W.-J.; Jiang, H.; Yu, H.-Q. Development of Biochar-Based Functional Materials: Toward a Sustainable Platform Carbon Material. *Chem. Rev.* **2015**, *115*, 12251–12285, doi:10.1021/acs.chemrev.5b00195.

66. Tan, X.; Liu, Y.; Zeng, G.; Wang, X.; Hu, X.; Gu, Y.; Yang, Z. Application of biochar for the removal of pollutants from aqueous solutions. *Chemosphere* **2015**, *125*, 70–85, doi:10.1016/J.CHEMOSPHERE.2014.12.058.

67. Chen, Y.; Zhang, X.; Chen, W.; Yang, H.; Chen, H. The structure evolution of biochar from biomass pyrolysis and its correlation with gas pollutant adsorption performance. *Bioresour. Technol.* **2017**, *246*, 101–109, doi:10.1016/j.biortech.2017.08.138.

68. Jimenez-Cordero, D.; Heras, F.; Alonso-Morales, N.; Gilarranz, M. A.; Rodriguez, J. J. Porous structure and morphology of granular chars from flash and conventional pyrolysis of grape seeds. *Biomass and Bioenergy* **2013**, *54*, 123–132, doi:10.1016/J.BIOMBIOE.2013.03.020.

69. Wafiq, A.; Reichel, D.; Hanafy, M. Pressure influence on pyrolysis product properties of raw and torrefied Miscanthus: Role of particle structure. *Fuel* **2016**, *179*, 156–167, doi:10.1016/J.FUEL.2016.03.092.

70. Cetin, E.; Moghtaderi, B. Effect of pyrolysis pressure and heating rate on radiata pine char structure and apparent gasification reactivity. *Fuel* **2005**, *84*, 1328–1334, doi:10.1016/J.FUEL.2004.07.016.

71. Fu, P.; Hu, S.; Xiang, J.; Sun, L.; Li, P.; Zhang, J.; Zheng, C. Pyrolysis of Maize Stalk on the Characterization of Chars Formed under Different Devolatilization Conditions. *Energy & Fuels* **2009**, *23*, 4605–4611, doi:10.1021/ef900268y.

72. Burhenne, L.; Damiani, M.; Aicher, T. Effect of feedstock water content and pyrolysis temperature on the structure and reactivity of spruce wood char produced in fixed bed pyrolysis. *Fuel* **2013**, *107*, 836–847, doi:10.1016/j.fuel.2013.01.033.

73. Chen, Y.; Yang, H.; Wang, X.; Zhang, S.; Chen, H. Biomass-based pyrolytic polygeneration system on cotton stalk pyrolysis: Influence of temperature. *Bioresour. Technol.* **2012**, *107*, 411–418, doi:10.1016/J.BIORTECH.2011.10.074.

74. Kim, K. H.; Kim, J.-Y.; Cho, T.-S.; Choi, J. W. Influence of pyrolysis temperature on physicochemical properties of biochar obtained from the fast pyrolysis of pitch pine (Pinus rigida). *Bioresour. Technol.* **2012**, *118*, 158–162, doi:10.1016/J.BIORTECH.2012.04.094.

75. Xin, S.; Yang, H.; Chen, Y.; Yang, M.; Chen, L.; Wang, X.; Chen, H. Chemical structure evolution of char during the pyrolysis of cellulose. *J. Anal. Appl. Pyrolysis* **2015**, *116*, 263–271, doi:10.1016/J.JAAP.2015.09.002.

76. Liu, Z.; Quek, A.; Kent Hoekman, S.; Balasubramanian, R. Production of solid biochar fuel from waste biomass by hydrothermal carbonization. *Fuel* **2013**, *103*, 943–949, doi:10.1016/j.fuel.2012.07.069.

77. Ahmad, M.; Rajapaksha, A. U.; Lim, J. E.; Zhang, M.; Bolan, N.; Mohan, D.; Vithanage, M.; Lee, S. S.; Ok, Y. S. Biochar as a sorbent for contaminant management in soil and water: A review. *Chemosphere* **2014**, *99*, 19–33, doi:10.1016/J.CHEMOSPHERE.2013.10.071.

78. Jain, A.; Balasubramanian, R.; Srinivasan, M. P. Hydrothermal conversion of biomass waste to activated carbon with high porosity: A review. *Chem. Eng. J.* **2016**, *283*, 789–805, doi:10.1016/j.cej.2015.08.014.

79. Bansal, R. C.; Donnet, J.-B.; Stoeckli, F. *Active carbon*; M. Dekker: New York, 1988; ISBN 9780824778422.

80. Gergova, K.; Galushko, A.; Petrov, N.; Minkova, V. Investigation of the porous structure of activated carbons prepared by pyrolysis of agricultural by-products in a stream of water vapor. *Carbon N. Y.* **1992**, *30*, 721–727, doi:10.1016/0008-6223(92)90154-O.

81. Rosas, J. M.; Bedia, J.; Rodríguez-Mirasol, J.; Cordero, T. HEMP-derived activated carbon fibers by

chemical activation with phosphoric acid. *Fuel* **2009**, *88*, 19–26, doi:10.1016/J.FUEL.2008.08.004.

82. Rosas, J. M.; Bedia, J.; Rodríguez-Mirasol, J.; Cordero, T. Preparation of Hemp-Derived Activated Carbon Monoliths. Adsorption of Water Vapor. *Ind. Eng. Chem. Res.* **2008**, *47*, 1288–1296, doi:10.1021/ie070924w.
83. Girgis, B. S.; El-Hendawy, A.-N. A. Porosity development in activated carbons obtained from date pits under chemical activation with phosphoric acid. *Microporous Mesoporous Mater.* **2002**, *52*, 105–117, doi:10.1016/S1387-1811(01)00481-4.
84. Martin, M. J.; Artola, A.; Balaguer, M. D.; Rigola, M. Activated carbons developed from surplus sewage sludge for the removal of dyes from dilute aqueous solutions. *Chem. Eng. J.* **2003**, *94*, 231–239, doi:10.1016/S1385-8947(03)00054-8.
85. Hasar, H. Adsorption of nickel(II) from aqueous solution onto activated carbon prepared from almond husk. *J. Hazard. Mater.* **2003**, *97*, 49–57, doi:10.1016/S0304-3894(02)00237-6.
86. Hayashi, J.; Kazehaya, A.; Muroyama, K.; Watkinson, A. P. Preparation of activated carbon from lignin by chemical activation. *Carbon N. Y.* **2000**, *38*, 1873–1878, doi:10.1016/S0008-6223(00)00027-0.
87. Tsai, W. .; Chang, C. .; Lin, M. .; Chien, S. .; Sun, H. .; Hsieh, M. . Adsorption of acid dye onto activated carbons prepared from agricultural waste bagasse by $ZnCl_2$ activation. *Chemosphere* **2001**, *45*, 51–58, doi:10.1016/S0045-6535(01)00016-9.
88. Deng, H.; Yang, L.; Tao, G.; Dai, J. Preparation and characterization of activated carbon from cotton stalk by microwave assisted chemical activation—Application in methylene blue adsorption from aqueous solution. *J. Hazard. Mater.* **2009**, *166*, 1514–1521, doi:10.1016/J.JHAZMAT.2008.12.080.
89. Gonzalez-Serrano, E.; Cordero, T.; Rodríguez-Mirasol, J.; Rodríguez, J. J. Development of Porosity upon Chemical Activation of Kraft Lignin with $ZnCl_2$. *Ind. Eng. Chem. Res.* **1997**, *36*, 4832–4838, doi:10.1021/ie970261q.
90. Bedia, J.; Monsalvo, V. M.; Rodriguez, J. J.; Mohedano, A. F. Iron catalysts by chemical activation of sewage sludge with $FeCl_3$ for CWPO. *Chem. Eng. J.* **2017**, *318*, 224–230, doi:10.1016/j.cej.2016.06.096.
91. Mohedano, A. F.; Monsalvo, V. M.; Bedia, J.; Lopez, J.; Rodriguez, J. J. Highly stable iron catalysts from sewage sludge for CWPO. *J. Environ. Chem. Eng.* **2014**, *2*, 2359–2364, doi:10.1016/j.jece.2014.01.021.
92. Zazo, J. A.; Bedia, J.; Fierro, C. M.; Pliego, G.; Casas, J. A.; Rodriguez, J. J. Highly stable Fe on activated carbon catalysts for CWPO upon $FeCl_3$ activation of lignin from black liquors. *Catal. Today* **2012**, *187*, 115–121, doi:10.1016/j.cattod.2011.10.003.
93. Rufford, T. E.; Hulicova-Jurcakova, D.; Zhu, Z.; Lu, G. Q. A comparative study of chemical treatment by $FeCl_3$, $MgCl_2$, and $ZnCl_2$ on microstructure, surface chemistry, and double-layercapacitance of carbons from waste biomass. *J. Mater. Res.* **2010**, *25*, 1451–1459, doi:10.1557/JMR.2010.0186.
94. Fu, K.; Yue, Q.; Gao, B.; Sun, Y.; Wang, Y.; Li, Q.; Zhao, P.; Chen, S. Physicochemical and adsorptive properties of activated carbons from Arundo donax Linn utilizing different iron salts as activating agents. *J. Taiwan Inst. Chem. Eng.* **2014**, *45*, 3007–3015, doi:10.1016/j.jtice.2014.08.026.
95. Lillo-Ródenas, M. .; Cazorla-Amorós, D.; Linares-Solano, A. Understanding chemical reactions between carbons and NaOH and KOH. *Carbon N. Y.* **2003**, *41*, 267–275, doi:10.1016/S0008-6223(02)00279-8.
96. Lillo-Ródenas, M. A.; Lozano-Castelló, D.; Cazorla-Amorós, D.; Linares-Solano, A. Preparation of activated carbons from Spanish anthracite - II. Activation by NaOH. *Carbon N. Y.* **2001**, *39*, 751–759, doi:10.1016/S0008-6223(00)00186-X.
97. Martins, A. C.; Pezoti, O.; Cazetta, A. L.; Bedin, K. C.; Yamazaki, D. A. S.; Bandoch, G. F. G.; Asefa, T.; Visentainer, J. V.; Almeida, V. C. Removal of tetracycline by NaOH-activated carbon produced from macadamia nut shells: Kinetic and equilibrium studies. *Chem. Eng. J.* **2015**, *260*, 291–299,

doi:10.1016/J.CEJ.2014.09.017.

98. Jang, H. M.; Yoo, S.; Choi, Y.-K.; Park, S.; Kan, E. Adsorption isotherm, kinetic modeling and mechanism of tetracycline on Pinus taeda-derived activated biochar. *Bioresour. Technol.* **2018**, *259*, 24–31, doi:10.1016/J.BIORTECH.2018.03.013.
99. Lozano-Castelló, D.; Lillo-Ródenas, M. A.; Cazorla-Amorós, D.; Linares-Solano, A. Preparation of activated carbons from Spanish anthracite - I. Activation by KOH. *Carbon N. Y.* **2001**, *39*, 741–749, doi:10.1016/S0008-6223(00)00185-8.
100. Ahmed, M. J.; Theydan, S. K. Microporous activated carbon from Siris seed pods by microwave-induced KOH activation for metronidazole adsorption. *J. Anal. Appl. Pyrolysis* **2013**, *99*, 101–109, doi:10.1016/j.jaap.2012.10.019.
101. Salman, J. M.; Hameed, B. H. Effect of preparation conditions of oil palm fronds activated carbon on adsorption of bentazon from aqueous solutions. *J. Hazard. Mater.* **2010**, *175*, 133–137, doi:10.1016/J.JHAZMAT.2009.09.139.
102. Fernandez-Ruiz, C.; Bedia, J.; Bonal, P.; Rodriguez, J. J.; Gómez-Sainero, L. M. Chloroform conversion into ethane and propane by catalytic hydrodechlorination with Pd supported on activated carbons from lignin. *Catal. Sci. Technol.* **2018**, *8*, 3926–3935, doi:10.1039/C8CY00461G.
103. Tascón, J. M. D. *Novel carbon adsorbents*; 1st ed.; Elsevier, 2012; ISBN 9780080977454.
104. Rodríguez-Reinoso, F.; Molina-Sabio, M. Textural and chemical characterization of microporous carbons. *Adv. Colloid Interface Sci.* **1998**, *76–77*, 271–294, doi:10.1016/S0001-8686(98)00049-9.
105. Patrick, J. W. *Porosity in carbons : characterization and applications*; Edward Arnold, 1995; ISBN 0340544732.
106. Sing, K. S. W. Reporting physisorption data for gas/solid systems with special reference to the determination of surface area and porosity (Recommendations 1984). *Pure Appl. Chem.* **1985**, *57*, 603–619, doi:10.1351/pac198557040603.
107. Brunauer, S.; Emmett, P. H.; Teller, E. Adsorption of Gases in Multimolecular Layers. *J. Am. Chem. Soc.* **1938**, *60*, 309–319, doi:10.1021/ja01269a023.
108. Lippens, B. C.; J.H., de B. Studies on pore systems in catalysts: V. The t method. *J. Catal.* **1965**, *4*, 319–323, doi:10.1016/0021-9517(65)90307-6.
109. Gregg, S. J.; Sing, K. S. W. *Adsorption, surface area, and porosity*; 2nd ed.; Academic Press: London ;;New York, 1982; ISBN 9780123009562.
110. Barrett, E. P.; Joyner, L. G.; Halenda, P. P. The Determination of Pore Volume and Area Distributions in Porous Substances. I. Computations from Nitrogen Isotherms. *J. Am. Chem. Soc.* **1951**, *73*, 373–380, doi:10.1021/ja01145a126.
111. Horváth, G.; Kawazoe, K. Method for the calculation of effective pore size distribution in molecular sieve carbon. *J. Chem. Eng. Japan* **1983**, *16*, 470–475, doi:10.1252/jcej.16.470.
112. Lozano-Castelló, D.; Cazorla-Amorós, D.; Linares-Solano, A. Usefulness of CO_2 adsorption at 273 K for the characterization of porous carbons. In *Carbon*; Pergamon, 2004; Vol. 42, pp. 1231–1236.
113. Gaffney, J. S.; Marley, N. A.; Jones, D. E. Fourier Transform Infrared (FTIR) Spectroscopy. In *Characterization of Materials*; John Wiley & Sons, Inc.: Hoboken, NJ, USA, 2012.
114. Barrios, V. A. E.; Méndez, J. R. R.; Aguilar, N. V. P.; Espinosa, G. A.; Rodríguez, J. L. D. FTIR - An Essential Characterization Technique for Polymeric Materials. In *Infrared Spectroscopy - Materials Science, Engineering and Technology*; InTech, 2012.
115. Biniak, S.; Szymański, G.; Siedlewski, J.; Świątkowski, A. The characterization of activated carbons with oxygen and nitrogen surface groups. *Carbon N. Y.* **1997**, *35*, 1799–1810, doi:10.1016/S0008-6223(97)00096-

1.

116. Bouchelta, C.; Medjram, M. S.; Bertrand, O.; Bellat, J.-P. Preparation and characterization of activated carbon from date stones by physical activation with steam. *J. Anal. Appl. Pyrolysis* **2008**, *82*, 70–77, doi:10.1016/J.JAAP.2007.12.009.
117. Yang, P.; Zhang, J.; Liu, D.; Liu, M.; Zhang, H.; Zhao, P.; Zhang, C. Facile synthesis of porous nitrogen-doped carbon for aerobic oxidation of amines to imines. *Microporous Mesoporous Mater.* **2018**, *266*, 198–203, doi:10.1016/j.micromeso.2018.03.002.
118. Szymański, G. S.; Karpiński, Z.; Biniak, S.; Świątkowski, A. The effect of the gradual thermal decomposition of surface oxygen species on the chemical and catalytic properties of oxidized activated carbon. *Carbon N. Y.* **2002**, *40*, 2627–2639, doi:10.1016/S0008-6223(02)00188-4.
119. Haydar, S.; Moreno-Castilla, C.; Ferro-García, M. A.; Carrasco-Marín, F.; Rivera-Utrilla, J.; Perrard, A.; Joly, J. P. Regularities in the temperature-programmed desorption spectra of CO_2 and CO from activated carbons. *Carbon N. Y.* **2000**, *38*, 1297–1308, doi:10.1016/S0008-6223(99)00256-0.
120. Boehm, H. P. Some aspects of the surface chemistry of carbon blacks and other carbons. *Carbon N. Y.* **1994**, *32*, 759–769, doi:10.1016/0008-6223(94)90031-0.
121. Schönherr, J.; Buchheim, J.; Scholz, P.; Adelhelm, P.; Schönherr, J.; Buchheim, J. R.; Scholz, P.; Adelhelm, P. Boehm Titration Revisited (Part I): Practical Aspects for Achieving a High Precision in Quantifying Oxygen-Containing Surface Groups on Carbon Materials. *C* **2018**, *4*, 21, doi:10.3390/c4020021.
122. Rivera-Utrilla, J.; Bautista-Toledo, I.; Ferro-García, M. A.; Moreno-Castilla, C. Activated carbon surface modifications by adsorption of bacteria and their effect on aqueous lead adsorption. *J. Chem. Technol. Biotechnol.* **2001**, *76*, 1209–1215, doi:10.1002/jctb.506.
123. Faria, P. C. .; Órfão, J. J. .; Pereira, M. F. . Adsorption of anionic and cationic dyes on activated carbons with different surface chemistries. *Water Res.* **2004**, *38*, 2043–2052, doi:10.1016/j.watres.2004.01.034.
124. Worch, E. *Adsorption Technology in Water Treatment*; DE GRUYTER: Berlin, Boston, 2012; ISBN 9783110240238.
125. Langmuir, I. The adsorption of gases on plane surfaces of glass, mica and platinum. *J. Am. Chem. Soc.* **1918**, *40*, 1361–1403, doi:10.1021/ja02242a004.
126. Freundlich, H. Über die Adsorption in Lösungen. *Zeitschrift für Phys. Chemie* **1907**, *57U*, 385–470, doi:10.1515/zpch-1907-5723.
127. Dubinin, M.M. and Radushkevich, L. V. The Equation of the Characteristic Curve of Activated Charcoal. *Proc. Acad. Sci. Phys. Chem. Sect.* **1947**, *55*, 331, doi:10.4236/ojs.2014.41001.
128. Sips, R. On the Structure of a Catalyst Surface. *J. Chem. Phys.* **1948**, *16*, 490–495, doi:10.1063/1.1746922.
129. Redlich, O.; Peterson, D. L. A Useful Adsorption Isotherm. *J. Phys. Chem.* **1959**, *63*, 1024–1024, doi:10.1021/j150576a611.
130. Toth, J. State Equations of the Solid-gas Interface Layers. *Acta Chim. Acad. Sci. Hung.* **1971**, *69*, 311–328.
131. Dubinin, M. M.; Astakhov, V. A. Development of Ideas of Volume Filling of Micropores during Adsorption of Gases and Vapours by Microporous Adsorbents .2. General Fundamentals of Theory of Gas and Vapour Adsorption on Zeolites. *Izv. Akad. Nauk Sssr-Seriya Khimicheskaya* **1971**, 11-.
132. *Adsorption Processes for Water Treatment and Purification*; Bonilla-Petriciolet, A., Mendoza-Castillo, D. I., Reynel-Ávila, H. E., Eds.; Springer International Publishing: Cham, 2017; ISBN 978-3-319-58135-4.
133. Leyva-Ramos, R.; Geankoplis, C. J. Model simulation and analysis of surface diffusion of liquids in porous solids. *Chem. Eng. Sci.* **1985**, *40*, 799–807, doi:10.1016/0009-2509(85)85032-6.
134. Largitte, L.; Pasquier, R. A review of the kinetics adsorption models and their application to the

adsorption of lead by an activated carbon. *Chem. Eng. Res. Des.* **2016**, *109*, 495–504, doi:10.1016/J.CHERD.2016.02.006.

135. Ho, Y. .; McKay, G. Pseudo-second order model for sorption processes. *Process Biochem.* **1999**, *34*, 451–465, doi:10.1016/S0032-9592(98)00112-5.
136. Low, M. J. D. Kinetics of Chemisorption of Gases on Solids. *Chem. Rev.* **1960**, *60*, 267–312, doi:10.1021/cr60205a003.
137. Eckenfelder, W. W. (William W. *Industrial water pollution control*; McGraw-Hill, 2000; ISBN 0070393648.
138. Noll, K. E.; Gounaris, V.; Hou, W. *Adsorption technology for air and water pollution control*; Lewis Publishers, 1992; ISBN 9780873713405.
139. Tan, K. L.; Hameed, B. H. Insight into the adsorption kinetics models for the removal of contaminants from aqueous solutions. *J. Taiwan Inst. Chem. Eng.* **2017**, *74*, 25–48, doi:10.1016/J.JTICE.2017.01.024.
140. Najafi Nobar, S.; Farooq, S. Experimental and modeling study of adsorption and diffusion of gases in Cu-BTC. *Chem. Eng. Sci.* **2012**, *84*, 801–813, doi:10.1016/J.CES.2012.05.022.
141. Chu, K. . Improved fixed bed models for metal biosorption. *Chem. Eng. J.* **2004**, *97*, 233–239, doi:10.1016/S1385-8947(03)00214-6.
142. Bohart, G. S.; Adams, E. Q. Some aspects of the behavior of charcoal with respect to chlorine. *J. Am. Chem. Soc.* **1920**, *42*, 523–544, doi:10.1021/ja01448a018.
143. Cooney, D. O. *Adsorption design for wastewater treatment*; Lewis Publishers, 1999; ISBN 1566703336.
144. Thomas, H. C. Heterogeneous Ion Exchange in a Flowing System. *J. Am. Chem. Soc.* **1944**, *66*, 1664–1666, doi:10.1021/ja01238a017.
145. Yoon, Y. H.; Nelson, J. H. Application of Gas Adsorption Kinetics I. A Theoretical Model for Respirator Cartridge Service Life. *Am. Ind. Hyg. Assoc. J.* **1984**, *45*, 509–516, doi:10.1080/15298668491400197.
146. Wolborska, A. Adsorption on activated carbon of p-nitrophenol from aqueous solution. *Water Res.* **1989**, *23*, 85–91, doi:10.1016/0043-1354(89)90066-3.
147. Hamdaoui, O. Removal of copper(II) from aqueous phase by Purolite C100-MB cation exchange resin in fixed bed columns: Modeling. *J. Hazard. Mater.* **2009**, *161*, 737–746, doi:10.1016/J.JHAZMAT.2008.04.016.
148. Reguyal, F.; Sarmah, A. K. Adsorption of sulfamethoxazole by magnetic biochar: Effects of pH, ionic strength, natural organic matter and 17α-ethinylestradiol. *Sci. Total Environ.* **2018**, *628–629*, 722–730, doi:10.1016/j.scitotenv.2018.01.323.
149. Greiner, B. G.; Shimabuku, K. K.; Summers, R. S. Influence of biochar thermal regeneration on sulfamethoxazole and dissolved organic matter adsorption. *Environ. Sci. Water Res. Technol.* **2018**, *4*, 169–174, doi:10.1039/C7EW00379J.
150. Zheng, H.; Wang, Z.; Zhao, J.; Herbert, S.; Xing, B. Sorption of antibiotic sulfamethoxazole varies with biochars produced at different temperatures. *Environ. Pollut.* **2013**, *181*, 60–67, doi:10.1016/j.envpol.2013.05.056.
151. Xie, M.; Chen, W.; Xu, Z.; Zheng, S.; Zhu, D. Adsorption of sulfonamides to demineralized pine wood biochars prepared under different thermochemical conditions. *Environ. Pollut.* **2014**, *186*, 187–194, doi:10.1016/j.envpol.2013.11.022.
152. Han, X.; Liang, C.; Li, T.; Wang, K.; Huang, H.; Yang, X. Simultaneous removal of cadmium and sulfamethoxazole from aqueous solution by rice straw biochar. *J. Zhejiang Univ. Sci. B* **2013**, *14*, 640–649, doi:10.1631/jzus.B1200353.
153. Ahmed, M. B.; Zhou, J. L.; Ngo, H. H.; Guo, W.; Johir, M. A. H.; Sornalingam, K. Single and competitive sorption properties and mechanism of functionalized biochar for removing sulfonamide antibiotics from

water. *Chem. Eng. J.* **2017**, *311*, 348–358, doi:10.1016/j.cej.2016.11.106.

154. Li, T.; Han, X.; Liang, C.; Shohag, M. J. I.; Yang, X. Sorption of sulphamethoxazole by the biochars derived from rice straw and alligator flag. *Environ. Technol.* **2015**, *36*, 245–253, doi:10.1080/09593330.2014.943299.
155. Liu, P.; Liu, W.-J.; Jiang, H.; Chen, J.-J.; Li, W.-W.; Yu, H.-Q. Modification of bio-char derived from fast pyrolysis of biomass and its application in removal of tetracycline from aqueous solution. *Bioresour. Technol.* **2012**, *121*, 235–240, doi:10.1016/J.BIORTECH.2012.06.085.
156. Jing, X.-R.; Wang, Y.-Y.; Liu, W.-J.; Wang, Y.-K.; Jiang, H. Enhanced adsorption performance of tetracycline in aqueous solutions by methanol-modified biochar. *Chem. Eng. J.* **2014**, *248*, 168–174, doi:10.1016/J.CEJ.2014.03.006.
157. Chen, T.; Luo, L.; Deng, S.; Shi, G.; Zhang, S.; Zhang, Y.; Deng, O.; Wang, L.; Zhang, J.; Wei, L. Sorption of tetracycline on H3PO4 modified biochar derived from rice straw and swine manure. *Bioresour. Technol.* **2018**, *267*, 431–437, doi:10.1016/J.BIORTECH.2018.07.074.
158. Tang, L.; Yu, J.; Pang, Y.; Zeng, G.; Deng, Y.; Wang, J.; Ren, X.; Ye, S.; Peng, B.; Feng, H. Sustainable efficient adsorbent: Alkali-acid modified magnetic biochar derived from sewage sludge for aqueous organic contaminant removal. *Chem. Eng. J.* **2018**, *336*, 160–169, doi:10.1016/J.CEJ.2017.11.048.
159. Wang, H.; Chu, Y.; Fang, C.; Huang, F.; Song, Y.; Xue, X. Sorption of tetracycline on biochar derived from rice straw under different temperatures. *PLoS One* **2017**, *12*, e0182776, doi:10.1371/journal.pone.0182776.
160. Wang, X.; Liu, N.; Liu, Y.; Jiang, L.; Zeng, G.; Tan, X.; Liu, S.; Yin, Z.; Tian, S.; Li, J.; Wang, X.; Liu, N.; Liu, Y.; Jiang, L.; Zeng, G.; Tan, X.; Liu, S.; Yin, Z.; Tian, S.; Li, J. Adsorption Removal of 17β-Estradiol from Water by Rice Straw-Derived Biochar with Special Attention to Pyrolysis Temperature and Background Chemistry. *Int. J. Environ. Res. Public Health* **2017**, *14*, 1213, doi:10.3390/ijerph14101213.
161. Dong, X.; He, L.; Hu, H.; Liu, N.; Gao, S.; Piao, Y. Removal of 17β-estradiol by using highly adsorptive magnetic biochar nanoparticles from aqueous solution. *Chem. Eng. J.* **2018**, *352*, 371–379, doi:10.1016/J.CEJ.2018.07.025.
162. Essandoh, M.; Kunwar, B.; Pittman, C. U.; Mohan, D.; Mlsna, T. Sorptive removal of salicylic acid and ibuprofen from aqueous solutions using pine wood fast pyrolysis biochar. *Chem. Eng. J.* **2015**, *265*, 219–227, doi:10.1016/j.cej.2014.12.006.
163. Salem, N. A.; Yakoot, S. M. Non-steroidal Anti-inflammatory Drug, Ibuprofen Adsorption Using Rice Straw Based Biochar. *Int. J. Pharmacol.* **2016**, *12*, 729–736, doi:10.3923/ijp.2016.729.736.
164. Lonappan, L.; Rouissi, T.; Kaur Brar, S.; Verma, M.; Surampalli, R. Y. An insight into the adsorption of diclofenac on different biochars: Mechanisms, surface chemistry, and thermodynamics. *Bioresour. Technol.* **2018**, *249*, 386–394, doi:10.1016/j.biortech.2017.10.039.
165. Tong, Y.; Mayer, B. K.; McNamara, P. J. Triclosan adsorption using wastewater biosolids-derived biochar. *Environ. Sci. Water Res. Technol.* **2016**, *2*, 761–768, doi:10.1039/C6EW00127K.
166. Kimbell, L. K.; Tong, Y.; Mayer, B. K.; McNamara, P. J. Biosolids-Derived Biochar for Triclosan Removal from Wastewater. *Environ. Eng. Sci.* **2018**, *35*, 513–524, doi:10.1089/ees.2017.0291.
167. Mandal, A.; Singh, N.; Purakayastha, T. J. Characterization of pesticide sorption behaviour of slow pyrolysis biochars as low cost adsorbent for atrazine and imidacloprid removal. *Sci. Total Environ.* **2017**, *577*, 376–385, doi:10.1016/J.SCITOTENV.2016.10.204.
168. Cao, X.; Harris, W. Properties of dairy-manure-derived biochar pertinent to its potential use in remediation. *Bioresour. Technol.* **2010**, *101*, 5222–5228, doi:10.1016/J.BIORTECH.2010.02.052.

169. Zhao, X.; Ouyang, W.; Hao, F.; Lin, C.; Wang, F.; Han, S.; Geng, X. Properties comparison of biochars from corn straw with different pretreatment and sorption behaviour of atrazine. *Bioresour. Technol.* **2013**, *147*, 338–344, doi:10.1016/J.BIORTECH.2013.08.042.

170. Zhang, P.; Sun, H.; Yu, L.; Sun, T. Adsorption and catalytic hydrolysis of carbaryl and atrazine on pig manure-derived biochars: Impact of structural properties of biochars. *J. Hazard. Mater.* **2013**, *244–245*, 217–224, doi:10.1016/J.JHAZMAT.2012.11.046.

171. Xiao, F.; Pignatello, J. J. π+-π Interactions between (hetero)aromatic amine cations and the graphitic surfaces of pyrogenic carbonaceous materials. *Environ. Sci. Technol.* **2015**, *49*, 906–914, doi:10.1021/es5043029.

172. Liu, N.; Charrua, A. B.; Weng, C.-H.; Yuan, X.; Ding, F. Characterization of biochars derived from agriculture wastes and their adsorptive removal of atrazine from aqueous solution: A comparative study. *Bioresour. Technol.* **2015**, *198*, 55–62, doi:10.1016/J.BIORTECH.2015.08.129.

173. Cederlund, H.; Börjesson, E.; Lundberg, D.; Stenström, J. Adsorption of Pesticides with Different Chemical Properties to a Wood Biochar Treated with Heat and Iron. *Water, Air, Soil Pollut.* **2016**, *227*, 203, doi:10.1007/s11270-016-2894-z.

174. Sun, K.; Jin, J.; Keiluweit, M.; Kleber, M.; Wang, Z.; Pan, Z.; Xing, B. Polar and aliphatic domains regulate sorption of phthalic acid esters (PAEs) to biochars. *Bioresour. Technol.* **2012**, *118*, 120–127, doi:10.1016/j.biortech.2012.05.008.

175. Jin, J.; Sun, K.; Wu, F.; Gao, B.; Wang, Z.; Kang, M.; Bai, Y.; Zhao, Y.; Liu, X.; Xing, B. Single-solute and bi-solute sorption of phenanthrene and dibutyl phthalate by plant- and manure-derived biochars. *Sci. Total Environ.* **2014**, *473–474*, 308–316, doi:10.1016/j.scitotenv.2013.12.033.

176. Ghaffar, A.; Ghosh, S.; Li, F.; Dong, X.; Zhang, D.; Wu, M.; Li, H.; Pan, B. Effect of biochar aging on surface characteristics and adsorption behavior of dialkyl phthalates. *Environ. Pollut.* **2015**, *206*, 502–509, doi:10.1016/j.envpol.2015.08.001.

177. Jing, F.; Pan, M.; Chen, J. Kinetic and isothermal adsorption-desorption of PAEs on biochars: effect of biomass feedstock, pyrolysis temperature, and mechanism implication of desorption hysteresis. *Environ. Sci. Pollut. Res.* **2018**, *25*, 11493–11504, doi:10.1007/s11356-018-1356-0.

178. Rajapaksha, A. U.; Vithanage, M.; Ahmad, M.; Seo, D.-C.; Cho, J.-S.; Lee, S.-E.; Lee, S. S.; Ok, Y. S. Enhanced sulfamethazine removal by steam-activated invasive plant-derived biochar. *J. Hazard. Mater.* **2015**, *290*, 43–50, doi:10.1016/J.JHAZMAT.2015.02.046.

179. Huang, L.; Wang, M.; Shi, C.; Huang, J.; Zhang, B. Adsorption of tetracycline and ciprofloxacin on activated carbon prepared from lignin with H3PO4activation. *Desalin. Water Treat.* **2014**, *52*, 2678–2687, doi:10.1080/19443994.2013.833873.

180. Fan, H.-T.; Shi, L.-Q.; Shen, H.; Chen, X.; Xie, K.-P. Equilibrium, isotherm, kinetic and thermodynamic studies for removal of tetracycline antibiotics by adsorption onto hazelnut shell derived activated carbons from aqueous media. *RSC Adv.* **2016**, *6*, 109983–109991, doi:10.1039/C6RA23346E.

181. Marzbali, M. H.; Esmaieli, M.; Abolghasemi, H.; Marzbali, M. H. Tetracycline adsorption by H3PO4-activated carbon produced from apricot nut shells: A batch study. *Process Saf. Environ. Prot.* **2016**, *102*, 700–709, doi:10.1016/J.PSEP.2016.05.025.

182. Li, G.; Zhang, D.; Wang, M.; Huang, J.; Huang, L. Preparation of activated carbons from Iris tectorum employing ferric nitrate as dopant for removal of tetracycline from aqueous solutions. *Ecotoxicol. Environ. Saf.* **2013**, *98*, 273–282, doi:10.1016/j.ecoenv.2013.08.015.

183. Sayğılı, H.; Güzel, F. Effective removal of tetracycline from aqueous solution using activated carbon

prepared from tomato (Lycopersicon esculentum Mill.) industrial processing waste. *Ecotoxicol. Environ. Saf.* **2016**, *131*, 22–29, doi:10.1016/J.ECOENV.2016.05.001.

184. Güzel, F.; Sayğılı, H. Adsorptive efficacy analysis of novel carbonaceous sorbent derived from grape industrial processing wastes towards tetracycline in aqueous solution. *J. Taiwan Inst. Chem. Eng.* **2016**, *60*, 236–240, doi:10.1016/j.jtice.2015.10.003.
185. Takdastan, A.; Mahvi, A. H.; Lima, E. C.; Shirmardi, M.; Babaei, A. A.; Goudarzi, G.; Neisi, A.; Heidari Farsani, M.; Vosoughi, M. Preparation, characterization, and application of activated carbon from low-cost material for the adsorption of tetracycline antibiotic from aqueous solutions. *Water Sci. Technol.* **2016**, *74*, 2349–2363, doi:10.2166/wst.2016.402.
186. Oliveira, G.; Calisto, V.; Santos, S. M.; Otero, M.; Esteves, V. I. Paper pulp-based adsorbents for the removal of pharmaceuticals from wastewater: A novel approach towards diversification. *Sci. Total Environ.* **2018**, *631–632*, 1018–1028, doi:10.1016/J.SCITOTENV.2018.03.072.
187. Moura, F. C. C.; Rios, R. D. F.; Galvão, B. R. L. Emerging contaminants removal by granular activated carbon obtained from residual Macauba biomass. *Environ. Sci. Pollut. Res.* **2018**, *25*, 26482–26492, doi:10.1007/s11356-018-2713-8.
188. Rovani, S.; Censi, M. T.; Pedrotti, S. L.; Lima, É. C.; Cataluña, R.; Fernandes, A. N. Development of a new adsorbent from agro-industrial waste and its potential use in endocrine disruptor compound removal. *J. Hazard. Mater.* **2014**, *271*, 311–320, doi:10.1016/J.JHAZMAT.2014.02.004.
189. To, M.-H.; Hadi, P.; Hui, C.-W.; Lin, C. S. K.; McKay, G. Mechanistic study of atenolol, acebutolol and carbamazepine adsorption on waste biomass derived activated carbon. *J. Mol. Liq.* **2017**, *241*, 386–398, doi:10.1016/J.MOLLIQ.2017.05.037.
190. Baccar, R.; Sarrà, M.; Bouzid, J.; Feki, M.; Blánquez, P. Removal of pharmaceutical compounds by activated carbon prepared from agricultural by-product. *Chem. Eng. J.* **2012**, *211–212*, 310–317, doi:10.1016/J.CEJ.2012.09.099.
191. Chakraborty, P.; Banerjee, S.; Kumar, S.; Sadhukhan, S.; Halder, G. Elucidation of ibuprofen uptake capability of raw and steam activated biochar of Aegle marmelos shell: Isotherm, kinetics, thermodynamics and cost estimation. *Process Saf. Environ. Prot.* **2018**, *118*, 10–23, doi:10.1016/J.PSEP.2018.06.015.
192. Mestre, A. S.; Pires, J.; Nogueira, J. M. F.; Carvalho, A. P. Activated carbons for the adsorption of ibuprofen. *Carbon N. Y.* **2007**, *45*, 1979–1988, doi:10.1016/J.CARBON.2007.06.005.
193. García-Mateos, F. J.; Ruiz-Rosas, R.; Marqués, M. D.; Cotoruelo, L. M.; Rodríguez-Mirasol, J.; Cordero, T. Removal of paracetamol on biomass-derived activated carbon: Modeling the fixed bed breakthrough curves using batch adsorption experiments. *Chem. Eng. J.* **2015**, *279*, 18–30, doi:10.1016/J.CEJ.2015.04.144.
194. Wong, S.; Lim, Y.; Ngadi, N.; Mat, R.; Hassan, O.; Inuwa, I. M.; Mohamed, N. B.; Low, J. H. Removal of acetaminophen by activated carbon synthesized from spent tea leaves: equilibrium, kinetics and thermodynamics studies. *Powder Technol.* **2018**, *338*, 878–886, doi:10.1016/J.POWTEC.2018.07.075.
195. Chen, D.; Xie, S.; Chen, C.; Quan, H.; Hua, L.; Luo, X.; Guo, L. Activated biochar derived from pomelo peel as a high-capacity sorbent for removal of carbamazepine from aqueous solution. *RSC Adv.* **2017**, *7*, 54969–54979, doi:10.1039/C7RA10805B.
196. Torrellas, S. Á.; García Lovera, R.; Escalona, N.; Sepúlveda, C.; Sotelo, J. L.; García, J. Chemical-activated carbons from peach stones for the adsorption of emerging contaminants in aqueous solutions. *Chem. Eng. J.* **2015**, *279*, 788–798, doi:10.1016/J.CEJ.2015.05.104.
197. Cunha, M. R.; Lima, E. C.; Cimirro, N. F. G. M.; Thue, P. S.; Dias, S. L. P.; Gelesky, M. A.; Dotto, G. L.;

dos Reis, G. S.; Pavan, F. A. Conversion of Eragrostis plana Nees leaves to activated carbon by microwave-assisted pyrolysis for the removal of organic emerging contaminants from aqueous solutions. *Environ. Sci. Pollut. Res.* **2018**, *25*, 23315–23327, doi:10.1007/s11356-018-2439-7.

198. Beltrame, K. K.; Cazetta, A. L.; de Souza, P. S. C.; Spessato, L.; Silva, T. L.; Almeida, V. C. Adsorption of caffeine on mesoporous activated carbon fibers prepared from pineapple plant leaves. *Ecotoxicol. Environ. Saf.* **2018**, *147*, 64–71, doi:10.1016/J.ECOENV.2017.08.034.
199. Sarıcı-Özdemir, Ç.; Önal, Y. Synthesis of new activated carbons produced from polymer waste. *Fullerenes, Nanotub. Carbon Nanostructures* **2018**, *26*, 451–457, doi:10.1080/1536383X.2018.1447930.
200. Lupul, I.; Yperman, J.; Carleer, R.; Gryglewicz, G. Adsorption of atrazine on hemp stem-based activated carbons with different surface chemistry. *Adsorption* **2015**, *21*, 489–498, doi:10.1007/s10450-015-9689-1.
201. Chang, K. L.; Shih, Y. H.; Tseng, C. H.; Chen, S. T.; Chen, C. C. Adsorption Studies on the Removal of an Herbicide (Atrazine) Using Activated Carbons Prepared from Agricultural Waste Sugarcane Bagasse. *Appl. Mech. Mater.* **2012**, *251*, 378–382, doi:10.4028/www.scientific.net/AMM.251.378.
202. Chaparadza, A.; Hossenlopp, J. M. Adsorption kinetics, isotherms and thermodynamics of atrazine removal using a banana peel based sorbent. *Water Sci. Technol.* **2012**, *65*, 940–947, doi:10.2166/wst.2012.935.
203. Mohsen Nourouzi, M.; Chuah, T. G.; Choong, T. S. Y. Adsorption of glyphosate onto activated carbon derived from waste newspaper. *Desalin. Water Treat.* **2010**, *24*, 321–326, doi:10.5004/dwt.2010.1461.
204. Salman, J. M. Batch Study for Insecticide Carbofuran Adsorption onto Palm-Oil-Fronds-Activated Carbon. *J. Chem.* **2013**, *2013*, 1–5, doi:10.1155/2013/630371.
205. Al Bahri, M.; Calvo, L.; Gilarranz, M. A.; Rodriguez, J. J. Activated carbon from grape seeds upon chemical activation with phosphoric acid: Application to the adsorption of diuron from water. *Chem. Eng. J.* **2012**, *203*, 348–356, doi:10.1016/J.CEJ.2012.07.053.
206. Bouhamidi, Y.; Kaouah, F.; Nouri, L.; Boumaza, S.; Trari, M.; Bendjama, Z. Kinetic, thermodynamic, and isosteric heat of dibutyl and diethyl phthalate removal onto activated carbon from Albizzia julibrissin pods. *Part. Sci. Technol.* **2018**, *36*, 235–243, doi:10.1080/02726351.2016.1243179.
207. Wang, Z.; Chen, L. Adsorption characteristics of dibutyl phthalate from aqueous solution using ginkgo leaves-activated carbon by chemical activation with zinc chloride. *Desalin. Water Treat.* **2015**, *54*, 1969–1980, doi:10.1080/19443994.2014.893207.
208. Fang, Z. Q.; Huang, H. J. Adsorption of Di-N-butyl Phthalate onto Nutshell-Based Activated Carbon. Equilibrium, Kinetics and Thermodynamics. *Adsorpt. Sci. Technol.* **2009**, *27*, 685–700, doi:10.1260/0263-6174.27.7.685.
209. Ahmed, M. B.; Zhou, J. L.; Ngo, H. H.; Johir, M. A. H.; Sornalingam, K. Sorptive removal of phenolic endocrine disruptors by functionalized biochar: Competitive interaction mechanism, removal efficacy and application in wastewater. *Chem. Eng. J.* **2018**, *335*, 801–811, doi:10.1016/J.CEJ.2017.11.041.
210. Mestre, A. S.; Pires, J.; Nogueira, J. M. F.; Parra, J. B.; Carvalho, A. P.; Ania, C. O. Waste-derived activated carbons for removal of ibuprofen from solution: Role of surface chemistry and pore structure. *Bioresour. Technol.* **2009**, *100*, 1720–1726, doi:10.1016/J.BIORTECH.2008.09.039.
211. Mondal, S.; Bobde, K.; Aikat, K.; Halder, G. Biosorptive uptake of ibuprofen by steam activated biochar derived from mung bean husk: Equilibrium, kinetics, thermodynamics, modeling and eco-toxicological studies. *J. Environ. Manage.* **2016**, *182*, 581–594, doi:10.1016/J.JENVMAN.2016.08.018.
212. Bedia, J.; Ruiz-Rosas, R.; Rodríguez-Mirasol, J.; Cordero, T. Kinetic study of the decomposition of 2-butanol on carbon-based acid catalyst. *AIChE J.* **2010**, *56*, 1557–1568, doi:10.1002/aic.12056.

213. Bedia, J.; Ruiz-Rosas, R.; Rodríguez-Mirasol, J.; Cordero, T. A kinetic study of 2-propanol dehydration on carbon acid catalysts. *J. Catal.* **2010**, *271*, 33–42, doi:10.1016/j.jcat.2010.01.023.

214. Jung, C.; Park, J.; Lim, K. H.; Park, S.; Heo, J.; Her, N.; Oh, J.; Yun, S.; Yoon, Y. Adsorption of selected endocrine disrupting compounds and pharmaceuticals on activated biochars. *J. Hazard. Mater.* **2013**, *263*, 702–710, doi:10.1016/J.JHAZMAT.2013.10.033.